Vladimir G. Petrov*, David Fellhauer, Xavier Gaona*, Kathy Dardenne, Jörg Rothe, Stepan N. Kalmykov and Marcus Altmaier

# Solubility and hydrolysis of Np(V) in dilute to concentrated alkaline NaCl solutions: formation of Na–Np(V)–OH solid phases at 22 °C

DOI 10.1515/ract-2016-2614
Received April 8, 2016; accepted July 18, 2016; published online August 30, 2016

**Abstract:** The solubility of Np(V) was investigated at $T = 22 \pm 2$ °C in alkaline NaCl solutions of different ionic strength (0.1–5.0 M). The solid phases controlling the solubility at different $-\log_{10} m_{H^+}$($pH_m$) and NaCl concentration were characterized by XRD, quantitative chemical analysis, SEM–EDS and XAFS (both XANES and EXAFS). Aqueous phases in equilibrium with Np(V) solids were investigated for selected samples within $8.9 \le pH_m \le 10.3$ by UV-vis/NIR absorption spectroscopy. In 0.1 M NaCl, the experimental solubility of the initial greenish $NpO_2OH$(am) solid phase is in good agreement with previous results obtained in $NaClO_4$ solutions, and is consistent with model calculations for fresh $NpO_2OH$(am) using the thermodynamic data selection in NEA–TDB. Below $pH_m \sim 11.5$ and for all NaCl concentrations studied, Np concentration in equilibrium with the solid phase remained constant during the timeframe of this study (~2 years). This observation is in contrast to the aging of the initial $NpO_2OH$(am) into a more crystalline modification with the same stoichiometry, $NpO_2OH$(am, aged), as reported in previous studies for concentrated $NaClO_4$ and NaCl. Instead, the greenish $NpO_2OH$(am) transforms into a white solid phase in those systems with [NaCl] ≥ 1.0 M and $pH_m \ge 11.5$, and into two different pinkish phases above $pH_m \sim 13.2$. The solid phase transformation is accompanied by a drop in Np solubility of 0.5–2 $\log_{10}$-units (depending upon NaCl concentration). XANES analyses of green, white and pink phases confirm the predominance of Np(V) in all cases. Quantitative chemical analysis shows the incorporation of $Na^+$ in the original $NpO_2OH$(am) material, with Na:Np ≤ 0.3 for the greenish solids and 0.8 ≤ Na:Np ≤ 1.6 for the white and pinkish phases. XRD data confirms the amorphous character of the greenish phase, whereas white and pink solids show well-defined but discrepant XRD patterns. Furthermore, the XRD pattern collected for one of the pink solid phases match the data recently reported for $NaNpO_2(OH)_2$(cr). UV-vis/NIR spectra collected in 0.1–5.0 M NaCl solutions show the predominance of $NpO_2^+$ (≥80%) at $pH_m \le 10.3$. This observation is consistent with the Np(V) hydrolysis scheme currently selected in the NEA–TDB. This work provides sound evidences on the formation of ternary Na–Np(V)–OH solid phases in Na-rich hyperalkaline solutions and ambient temperature conditions. Given the unexpectedly high complexity of the system, further experimental efforts dedicated to assess the thermodynamic properties of these solid phases are needed, especially in view of their likely relevance as solubility controlling Np(V) solid phases in Na-rich systems such as saline and cement-based environments in the context of the safety assessment for nuclear waste disposal.

**Keywords:** Np(V), solubility, hydrolysis, thermodynamic data, Na–Np(V)–OH solid phases.

***Corresponding authors: Vladimir G. Petrov,** Lomonosov Moscow State University, Department of Chemistry, 119991, Leninskie gory, 1 bld. 3, Moscow, Russia, E-mail: vladimir.g.petrov@gmail.com; and **Xavier Gaona**, Karlsruhe Institute of Technology, Institute for Nuclear Waste Disposal, P.O. Box 3640, 76021 Karlsruhe, Germany, E-mail: xavier.gaona@kit.edu
**David Fellhauer, Kathy Dardenne, Jörg Rothe and Marcus Altmaier:** Karlsruhe Institute of Technology, Institute for Nuclear Waste Disposal, P.O. Box 3640, 76021 Karlsruhe, Germany
**Stepan N. Kalmykov:** Lomonosov Moscow State University, Department of Chemistry, 119991, Leninskie gory, 1 bld. 3, Moscow, Russia; and NRC Kurchatov Institute, 123182, Akademika Kurchatova pl. 1, Moscow, Russia

## 1 Introduction

Neptunium-237 ($t_{1/2} = 2.14 \times 10^6$ years) is produced via neutron irradiation of $^{235}U$ in nuclear reactors, and is initially present at relatively low concentrations in spent nuclear fuel (SNF). In the context of high level waste disposal, $^{237}Np$ is considered as a relevant dose contributor in the long term due to its ingrowth in SNF by the $\alpha$ decay of $^{241}Am$ ($t_{1/2} = 432.2$ years). On the other hand, traces of neptunium present in the environment are mostly originating

from atmospheric testing of nuclear weapons. In addition, accidents and releases from weapons production and reprocessing facilities (i. e. Hanford and Mayak sites) are responsible for most of the localized neptunium (point source) contamination [1–3].

Investigations on Np solubility and speciation reported in the present study are relevant to reliably assess the maximum Np concentration in the aqueous phase in the near-field of a nuclear waste repository (so-called source term) due to a potential intrusion of water. The source term is a highly relevant factor in the performance assessment of a nuclear waste repository as it sets the upper limit concentration for the Np inventory potentially mobilized from a waste repository via an aqueous pathway.

Hydrolysis and carbonate complexation are the most relevant chemical reactions governing the chemical behavior of actinides (and metal cations in general) in the environment. A comprehensive overview on several aspects related to actinide and Np solubility and speciation in aqueous media has been previously reported elsewhere [4–6]. Although in some cases kinetic factors can strongly hinder this type of reaction, solution thermodynamics remains as a very accurate approach to describe hydrolysis and solubility phenomena under given pH and ionic strength conditions. The thermochemical database project (TDB) of the Nuclear Energy Agency (NEA) comprises a comprehensive selection of equilibrium constants and parameters currently available for actinides and fission products in aqueous solutions and is widely recognized as the most authoritative source of thermodynamic data for radionuclides and other elements relevant in the field of nuclear waste disposal, e. g. Fe [7–13]. Based on the NEA–TDB, it is predicted that Np(IV) will be the dominant redox state under the reducing conditions expected to prevail in deep geological repositories. On the other hand, Np(V) will dominate the chemistry of neptunium under anoxic to oxidizing redox conditions as those expected in the biosphere or in the early stage of a repository closure. Np(IV) sorbs very strongly to many mineral surfaces [14–17] and forms sparingly soluble oxyhydroxides over a wide pH-range [8], whereas Np(V) generally has a significantly lower tendency towards sorption (except under hyper-alkaline pH conditions) [16, 18–22] and has much higher equilibrium solubility concentrations at many repository relevant pH conditions. In this framework, an accurate knowledge of the aqueous Np(V) species prevailing in solution as well as the solid Np(V) phases controlling the maximum solubility is required for the understanding of the chemical behavior of neptunium in the context of a deep geological disposal.

All available experimental studies (until 2003) dealing with Np(V) hydrolysis and solubility were critically reviewed within the NEA–TDB project [7, 8]. Although the use of different experimental approaches was reported (potentiometric titrations, spectrophotometry, solubility, electro migration, paper-electrophoresis, etc.) ([23–29], among others), the final thermodynamic data selection included the first and second hydrolysis constants of Np(V), and mostly relied on the solubility study by Neck and co-workers [28] conducted over uncharacterized $NpO_2OH(am)$. The uncertainty assigned to the second hydrolysis constant ($\log_{10} {}^{*}\beta^{\circ}_{(1,2)}$) was increased, to be consistent with the solubility study by Itagaki and co-workers [27], also conducted over $NpO_2OH(am)$. The NEA–TDB review in [7] already acknowledged that the hydrolysis constants derived from solubility measurements with uncharacterized $NpO_2OH(am)$ should be accepted only with considerable caution, and encouraged new experimental efforts dedicated to tackle these uncertainties. In a posterior and very comprehensive study conducted by Rao and co-workers, the hydrolysis of Np(V) was investigated in TMA–OH solutions combining potentiometric, spectroscopic and calorimetric techniques [30]. The stability constants derived in [30] differed significantly from those selected in the NEA–TDB, leading to a so far unsolved discussion on the validity of the current chemical and thermodynamic models for Np(V) [31, 32]. Relevant experimental shortcomings were identified in both investigations. In the potentiometric and spectroscopic study by Rao and co-workers, the presence of carbonate and the possible formation of Np(V)–$CO_3$ aqueous species was suspected based on the NIR absorption bands at 991 and 1020 nm. Provided the lack of solid phase characterization in the solubility study by Neck and co-workers [28], Rao and co-workers proposed a new chemical model for the interpretation of the solubility data with $NaNpO_2(OH)_2(s)$ as solubility-controlling phase and consistent with the hydrolysis scheme derived in [30]. Indeed, the formation of ternary Na–Np(V)–OH solid phases in concentrated NaOH solutions under hydrothermal conditions but also at room temperature has been described by a number of authors [33–37]. Recently, Fellhauer and co-workers investigated the solubility of Np(V) at $T = 22 \pm 2\,^{\circ}C$ in dilute to concentrated alkaline $CaCl_2$ solutions [38, 39]. Sparingly soluble ternary Ca–Np(V)–OH and quaternary Ca–Np(V)–OH–Cl solid phases were found to control the solubility of Np within the investigated $pH_m$-range (8–12) and $CaCl_2$ concentrations (0.25–4.5 M). The authors observed also the formation of very stable ternary $Ca_xNpO_2(OH)_y^{1+2x-y}$ species in the aqueous phase ($x = 1$ and 3; $y = 2$ and 5), in line with previous studies available for An(III) and An(IV)

in alkaline $CaCl_2$ solutions [40–42]. No further experimental studies dedicated to shed light on the relevant topic of Np(V) solubility and hydrolysis in NaCl systems have been reported after the discussion between Neck and Rao.

NaCl is a common background electrolyte in the biosphere (e. g. ~0.5 M in sea water), but also in the context of nuclear waste disposal where NaCl-dominated salt brines (up to 5 M NaCl) are expected to form in the unlikely event of water intrusion into a salt-rock based repository. Cementitious wasteforms and the use of cement based materials as construction materials in nuclear waste repositories are planned in several countries for the disposal of low and intermediate level wastes. This will result in aqueous systems characterized by hyperalkaline pH conditions and presence of rather high $Na^+$ and $K^+$ concentrations (~0.1 and ~0.2 M, respectively) in the early stage of cement degradation even in low ionic strength solutions.

In this work, undersaturation solubility experiments in dilute to concentrated NaCl solutions were performed at 22 ± 2 °C to assess the thermodynamic properties of Np(V) hydrolysis species and solid compounds forming in near-neutral to hyperalkaline pH conditions. Special emphasis was put on the identification of the solid phases controlling the solubility of Np(V) under the investigated pH and ionic strength conditions, which were characterized by XRD, SEM–EDS, quantitative chemical analysis and XAFS techniques. A significant effort was also dedicated to assess the presence of carbonate in the investigated systems, and to evaluate the possible formation of Np(V)–carbonate aqueous species and solid compounds.

# 2 Experimental

## 2.1 Chemicals

All reagents used in this study were of analytical grade. NaOH (Titrisol®), HCl (Titrisol®) and NaCl were obtained from Merck. Carbonate impurities in fresh 1.0 M NaOH (Titrisol) were quantified as $(3 \pm 1) \times 10^{-5}$ M using a Shimadzu TOC5000 equipment. All solutions were prepared with ultrapure water purified with a Milli-Q-academic (Millipore) apparatus and purged with Ar before use. All solutions and samples were prepared and handled inside an inert gas (Ar) glovebox at 22 ± 2 °C.

About 1.5 g of $^{237}Np$ were purified from trace impurities of Pu and Am using an ion exchange method [43]. The resulting oxidation state pure Np(V) stock solution (0.32 M $^{237}Np$ in 0.01 M HCl) was characterized by inductively-coupled plasma mass spectrometry (ICP–MS), $\gamma$ spectrometry, liquid scintillation counting (LSC), UV-vis/NIR and $\alpha$ spectrometry, which confirmed both the chemical and radiochemical purity of the $^{237}Np$ stock solution.

## 2.2 Solid phase preparation and solubility experiments

Aliquots of the Np stock solution were precipitated in dilute NaOH at pH ~11.5. The resulting greenish $NpO_2OH(am)$ was washed twice with Milli-Q water and diluted NaOH, and the supernatant replaced with NaCl–NaOH solutions of different ionic strength (0.1, 1.0, 3.0 and 5.0 M, or conversely 0.10, 1.02, 3.20 and 5.61 m, $mol \cdot kg_w^{-1}$) resulting in a total of 36 independent batch samples adjusted to different proton concentrations. The inventory of $^{237}Np$ in each sample was ~2 mg.

Samples were equilibrated for up to 2 years and systematically monitored for pH and [Np]. The aqueous concentration of Np was measured after 10 kD (~2–3 nm) ultrafiltration (Pall Life Sciences) by liquid scintillation counting (LSC) with a 1220 Quantulus instrument (Perkin Elmer). A small volume of the filtered sample (50–100 µL) was acidified with 2% $HNO_3$ and mixed with 10 mL of LSC–cocktail Ultima Gold XR (Perkin–Elmer); $\alpha$-radiation resulting from the decay of $^{237}Np$ was measured after $\alpha/\beta$-discrimination of the counts from the daughter nuclide $^{233}Pa$. Neptunium concentrations measured in molar units (M) were converted to molal scale (m) using the conversion factors reported for NaCl solutions in the NEA–TDB [8]. Three additional Np(V) samples in 5.0 M NaCl available from a previous study aged for ~6 years were analyzed following the same protocol as described above.

Selected samples with $pH_m \leq 10.3$ and $m_{Np} \geq 3 \times 10^{-6}$ m were centrifuged in a glovebox at 4020 *g* to remove suspended solid phase particles, and UV-vis/NIR spectra of the supernatant solutions (2 mL) recorded at 400 nm $\leq \lambda \leq$ 1200 nm with a high-resolution UV-vis/NIR spectrometer (Cary 5, Varian, USA). A second spectrum was recorded after addition of 20 µL 1 M HCl to a respective UV-vis/NIR sample aliquot in the cuvette (resulting $pH_m \approx 2$). Differences in the prominent NIR peak of Np(V) at $\lambda$ = 980–981 nm (corresponding to $NpO_2^+$) between both measurements were attributed to the presence of Np(V) hydrolysis species in the alkaline aliquot.

The proton concentration (molal scale, $pH_m = -\log_{10} m_{H^+}$) was measured using a combination pH electrode (type ROSS, Orion) calibrated against standard pH buffers (pH 8–13, Merck). At elevated ionic strengths, the measured pH ($pH_{exp}$) is an operational apparent value related to $m_{H^+}$ by the expression $pH_m = pH_{exp} + A_m$, where $A_m$ is an empirical

factor entailing the real activity coefficient of $H^+$ and the liquid junction potential of the combination electrode for a given NaCl concentration [44]. In NaCl–NaOH solutions with $m_{OH^-} > 0.03$ m, the $H^+$ concentration was calculated from the given $m_{OH^-}$ and the conditional ion product of water.

## 2.3 Solid phase characterization

The solubility samples listed in Table 1 are a representative set covering different ionic strength and pH conditions and were selected for exhaustive solid phase characterization based on different experimental methods. In these 13 samples, the solid phase was separated from the supernatant solution by centrifugation at 4020 *g* and washed five times with ethanol to remove traces of NaCl background electrolyte. The largest fraction of the resulting material was resuspended in ethanol and placed on a capped silicon single crystal sample holder (Dome, Bruker) in the glovebox under inert Ar atmosphere. XRD spectra of the neptunium solids were collected with a D8 Advance diffractometer (Bruker) in the $2\theta$ angle range 5–60°. Afterwards, the solid XRD sample was dissolved in 2% $HNO_3$ and analyzed for neptunium and sodium content by LSC and inductively coupled plasma optical emission spectrometry (ICP–OES, Optima 2000 by Perkin Elmer), respectively.

A fraction of the washed solid phase was separated and characterized by scanning electron microscope – energy disperse spectrometry (SEM–EDS). SEM images were obtained with a CamScan CS 44 FE (Cambridge Instruments) at an accelerating voltage of 15 kV. Energy-dispersive X-ray spectra were collected in several spots of the sample surface, and the atomic composition determined for Np, Na and Cl.

Selected solid samples were further investigated by XAFS at the INE-Beamline for Actinide Research at ANKA [45]. For these measurements, a suspension with ~1 mg of the solid material was transferred to a 400 µL polyethylene vial and centrifuged for 10 min at 4020 *g*. The centrifuge vial was then mounted in a gas-tight cell inside the Ar-glovebox and transported to the beamline. XAFS measurements were conducted under Ar atmosphere.

A tuneable monochromatic beam was delivered by the Ge(422) crystal pair in the Lemonnier-type double crystal monochromator (DCM). Higher harmonics were rejected from the two mirrors in the optics of the INE-Beamline by detuning the second crystal at a constant, controlled 70% from the rocking curve maximum [46]. Neptunium $L_{III}$ spectra were recorded at room temperature in fluorescence mode using a LE–Ge 5 element detector (Canberra-Eurisys). All Np spectra were calibrated in energy with the first inflection point in the XANES spectra of a Zr foil (17.998 keV), which was measured simultaneously.

XANES/EXAFS data treatment and analysis were performed with the ATHENA/ARTEMIS package following standard procedures [47, 48]. Scattering amplitude and phase shift data calculation to fit EXAFS data of white solids was based on the structure of $Na_2U_2O_7$(cr) [49] with the substitution of the central U atom by Np. The structure of $NaNpO_2(OH)_2$(cr) [37] was considered for the fit of the pinkish solids from the highest pH. Alternatively, single path scattering files for phase and amplitude were used in those cases where none of the previous options led to a stable fit. All fits were performed in the *R*-space with $k^2$-weighted data. For those samples with positive match with a crystalline structure, the available structural information was considered in the fit and thus the coordination number fixed to the expected value and $S_0^2$ allowed varying. On the contrary, coordination numbers

**Table 1:** Summary of samples and experimental methods used in this study for the characterization of neptunium solid phases.

| Sample | Ionic strength [M] | $pH_m$ | Color | XRD | SEM–EDS | CA | XANES | EXAFS |
|---|---|---|---|---|---|---|---|---|
| 1 | 0.1 | 9.4 | Green | – | – | – | ✓ | – |
| 2 | 0.1 | 10.6 | Green | ✓ | ✓ | ✓ | – | ✓ |
| 3 | 0.1 | 11.6 | Green | ✓ | ✓ | ✓ | – | – |
| 4 | 0.1 | 12.5 | Green | ✓ | ✓ | ✓ | – | ✓ |
| 5 | 1.0 | 10.3 | Green | ✓ | ✓ | ✓ | – | – |
| 6 | 1.0 | 11.8 | White | ✓ | ✓ | ✓ | – | – |
| 7 | 1.0 | 13.3 | Violet-pink | ✓ | ✓ | ✓ | ✓ | ✓ |
| 8 | 3.0 | 10.6 | Green | ✓ | ✓ | – | ✓ | – |
| 9 | 3.0 | 12.1 | White | ✓ | ✓ | ✓ | ✓ | ✓ |
| 10 | 5.0 | 9.6 | Green | – | – | – | ✓ | ✓ |
| 11 | 5.0 | 11.2 | Green | ✓ | ✓ | – | ✓ | ✓ |
| 12 | 5.0 | 12.6 | White | ✓ | ✓ | ✓ | ✓ | ✓ |
| 13 | 5.0 | 14.4 | Violet-pink | ✓ | ✓ | ✓ | – | ✓ |

were left free and $S_0^2$ was fixed to 1 in the case of amorphous phases.

# 3 Results and discussion

## 3.1 Solubility of Np(V) in NaCl solutions

Neptunium(V) solubility data determined in this work in 0.1, 1.0, 3.0 and 5.0 M NaCl solutions are summarized in Figure 1. The figure also shows previously reported solubility data of Np(V) in 0.1–3.0 M $NaClO_4$ [28], 0.98 M $NaClO_4$ [50], 1.0–5.0 M NaCl [51] and 5.0 M NaCl [29], as well as solubility data of Am(V) in 5.0 M NaCl [29]. Experimental data are compared with thermodynamic calculations considering $\log_{10} {}^*K^\circ_{s,0}(NpO_2OH(am, fresh))$, Np(V) hydrolysis constants and corresponding SIT ion interaction coefficients reported in the NEA–TDB [8].

A very good agreement is observed between Np(V) solubility data in 0.1 M NaCl (present work) and 0.1 M $NaClO_4$ systems [28]. Both datasets show also an excellent agreement with thermodynamic calculations using the NEA–TDB. Three well-defined regions are observed with slopes (log $m_{Np}$ vs. $pH_m$) of –1 ($9 \le pH_m \le 11$), 0 ($11 \le pH_m \le 12.1$) and +1 ($12.1 \le pH_m \le 12.8$). Neck and co-workers interpreted this behavior according with the solubility reactions (1)–(3). The same chemical model was afterwards selected by the NEA–TDB.

$$NpO_2OH(am, fresh) + H^+ \Leftrightarrow NpO_2^+ + H_2O \quad (1)$$

$$NpO_2OH(am, fresh) \Leftrightarrow NpO_2OH(aq) \quad (2)$$

$$NpO_2OH(am, fresh) + H_2O \Leftrightarrow NpO_2(OH)_2^- + H^+ \quad (3)$$

Within the timeframe of this study (2 years), no aging of the freshly precipitated $NpO_2OH(am, fresh)$ phase was

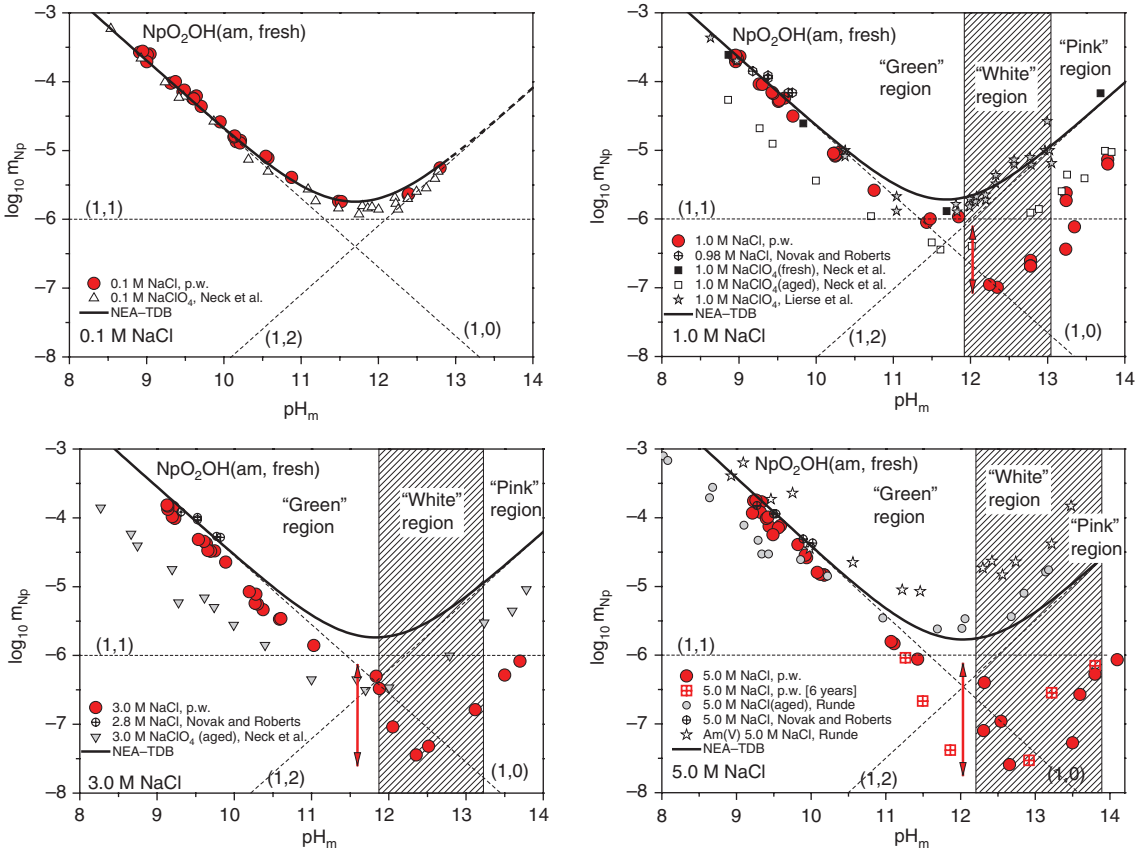



**Figure 1:** Solubility of Np(V) in 0.1, 1.0, 3.0 and 5.0 M NaCl ($m_{NaCl}$ = 0.10, 1.02, 3.20 and 5.61 m): experimental data (molal scale) and SIT model calculation (thick lines) based on the current NEA–TDB thermodynamic data selection. Dashed lines show the Np(V) aqueous speciation underlying the solubility of $NpO_2OH(am, fresh)$. "Green", "white" and "pink" regions correspond to the observed color of the solid phase in equilibrium with the supernatant. Experimental solubility data of Np(V) in 0.1–3.0 M $NaClO_4$ [28], 1.0 M $NaClO_4$ [50], 1.0–5.0 M NaCl [51] and 5.0 M NaCl [29], as well as solubility data of Am(V) in 5.0 M NaCl [29] appended in the figure for comparison.

observed for $pH_m \leq 11.5$ in any of the investigated NaCl systems. This observation is in disagreement with previously reported solubility data in concentrated $NaClO_4$ and NaCl (≥1.0 M, [28, 29]), where the aging of the initial solid phase and the consequent decrease in Np(V) concentration took place within a very short timeframe (few hours to few days). Note that the observations reported in [28] and [29] were considered in the review by [7] for the definition of a new solid phase, $NpO_2OH$(am, aged), with a $\log_{10} {}^{*}K^{\circ}_{s,0}$ 0.6 $\log_{10}$-units lower than the value selected for $NpO_2OH$(am, fresh).

A solid phase transformation occurs in our samples above $pH_m \sim 11.5$ and $I \geq 1.0$ M NaCl, where the original greenish phase converts into a white solid over several weeks to months. This is accompanied by a significant decrease in the Np solubility (0.5–2 $\log_{10}$-units) with respect to experimental data in $NaClO_4$ systems and thermodynamic calculations with $NpO_2OH$(am, fresh). A similar decrease in solubility was observed for those samples aged 6 years. The drop in solubility is more pronounced at elevated NaCl concentrations, thus hinting to the formation of a Na-bearing solid phase. Such a solid phase transformation and abrupt decrease in solubility was not observed in any of the previous solubility studies conducted at $I \geq 1.0$ M NaCl or $NaClO_4$ [28, 29, 50–52]. Note that all these studies considered significantly shorter equilibration time and greater $^{237}$Np inventory than in the present work [50]: $t_{eq} = 2$ days, ~1 g $^{237}$Np; [28]: $t_{eq} = 1$ day to 4 weeks, 10–30 mg $^{237}$Np; [51] and [52]: $t_{eq} = 37$ days, ~8 mg $^{237}$Np; [29]: $t_{eq}$ = several weeks, unreported $^{237}$Np inventory; present work: $t_{eq} = 2$ years, ~2 mg $^{237}$Np. In view of the observations gained in this work, we hypothesize that the equilibration time considered in previous studies was insufficient to allow the complete transformation of the original $NpO_2OH$(am) material, which remained as solubility-controlling phase in the system.

The further increase of $pH_m$ (above 13–13.5, depending upon NaCl concentration) results in the relatively fast transformation of the white phase to a violet-pinkish solid within few days. The solubility of both solid phases (white and violet-pink) increases steadily with $pH_m$ with a slope of +1 to +2 at $pH_m \geq 12.5$. The increase in solubility is well-reproduced in those samples aged 6 years.

## 3.2 Aqueous speciation by UV-vis/NIR

In order to get more information about the aqueous Np(V) equilibrium speciation, supernatant solutions of selected solubility samples with a sufficient Np concentration level (i. e. the least alkaline samples with $pH_m \leq 10.3$, see Table 2) were analysed by vis/NIR absorption spectroscopy. Figure 2 shows the relevant NIR region of the UV-vis/NIR spectra recorded for the untreated alkaline samples in 0.1–5.0 M NaCl ($pH_m = 8.9$–10.3) and the corresponding aliquots after addition of 20 µL 1 M HCl (resulting $pH_m \sim 2$). All spectra are very similar to the one reported for the unhydrolysed Np(V) aquo ion, $NpO_2(OH_2)_5^+$, in non-complexing 2 M $HClO_4$ [53] with its characteristic absorbance at $\lambda = 980.2$ nm ($\varepsilon = 395$ L · mol$^{-1}$ cm$^{-1}$). The slight deviations in the spectral features observed are due to contributions from Np(V) chloro complexes, $NpO_2(OH_2)_{5-n}Cl_n^{1-n}$, and Np(V) hydrolysis species, $NpO_2(OH_2)_{5-m}(OH)_m^{1-m}$, and are discussed in the following.

**Table 2:** Overview of the solubility samples studied by vis/NIR absorption spectroscopy.

| Sample | Ionic strength [M] | $pH_m$ | ΔAbs at 980nm (%) | Spectral features of acidified aliquots (mean values) | | |
|---|---|---|---|---|---|---|
| | | | | $\lambda_{max}$ (nm) | FWHM (nm) | $\varepsilon$ (M$^{-1}$ · cm$^{-1}$) |
| 1 | 0.1 | 8.93 | 1 | 980.2 | 7.4 | 384 ± 6 |
| 2 | 0.1 | 9.48 | 4 | | | |
| 3 | 0.1 | 10.14 | 15 | | | |
| 4 | 1.0 | 8.98 | 1 | 980.2 | 7.5 | 381 ± 17 |
| 5 | 1.0 | 9.43 | 5 | | | |
| 6 | 1.0 | 10.26 | 21 | | | |
| 7 | 3.0 | 9.18 | 1 | 980.4 | 7.9 | 374 ± 15 |
| 8 | 3.0 | 9.57 | 4 | | | |
| 9 | 3.0 | 10.24 | 18 | | | |
| 10 | 5.0 | 9.27 | 1 | 981.0 | 8.5 | 358 ± 15 |
| 11 | 5.0 | 9.41 | 2 | | | |
| 12 | 5.0 | 9.93 | 7 | | | |

The total concentration of Np(V) hydrolysis species under the alkaline conditions is estimated by evaluating the differences in the prominent NIR peak of Np(V) at $\lambda$ = 980–981 nm (corresponding to unhydrolysed Np(V) species) before and after acidification of the vis/NIR aliquot with HCl. Spectral features of the prominent Np(V) absorbance in the acidified aliquots are listed in the right part.

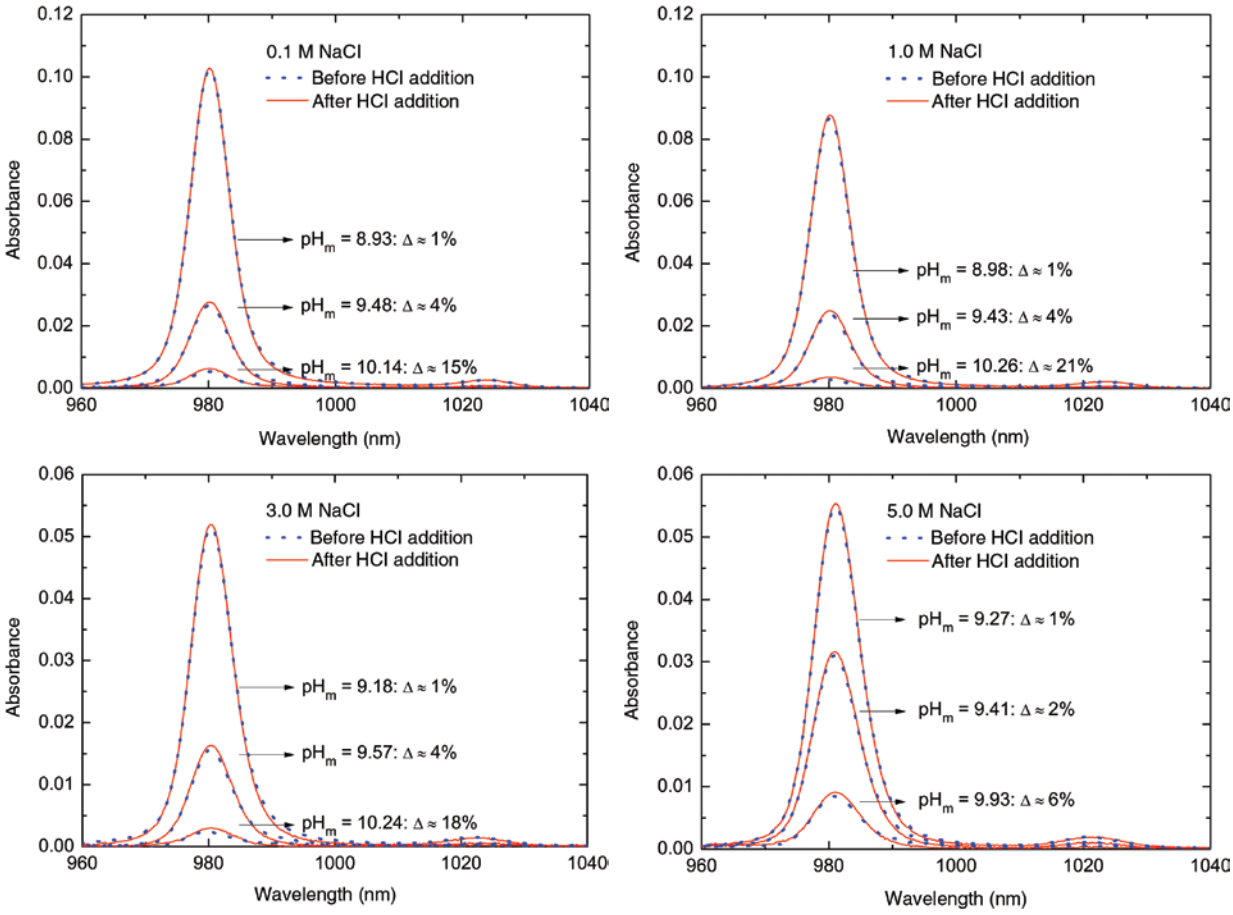



**Figure 2:** Near-IR absorption spectra of the saturated, supernatant solutions in equilibrium with $NpO_2OH$(am, fresh) in 0.1, 1.0, 3.0 and 5.0 M NaCl ($m_{NaCl}$ = 0.10, 1.02, 3.20 and 5.61 m). The vis/NIR sample aliquots were acidified in the cuvette with HCl after the measurement, and a second spectrum recorded. The total contribution of Np(V) hydrolysis species is estimated from the difference of the main peaks' heights ("Δ") in both spectra.

The impact and relevance of Np(V) chloro complexes in [NaCl] ≤ 5 M can be obtained from the spectra of the acidified sample aliquots ($pH_m \approx 2$) where contributions of Np(V) hydrolysis species are negligible. Spectral features of the prominent Np(V) peak are listed in Table 2. Up to the maximum chloride concentration (5.0 M), only small changes are observed: with increasing [$Cl^-$], $\lambda_{max}$ is shifted from 980.2 nm to 981.0 nm, FWHM increases from 7.4 to 8.5 nm, and the extinction coefficient decreases from $\varepsilon$ = 384–358 $L \cdot mol^{-1} \cdot cm^{-1}$ (the uncertainty of the $\varepsilon$ values is about ±20, corresponding to an absolute analytical error of 5% in the LSC determination of [Np]). Similar results for Np(V) in NaCl and LiCl solutions were reported in [54] and [55], respectively. The slight changes indicate a rather small contribution of Np(V) innersphere chloro species. This is supported by the EXAFS study of Np(V) in 3–10 M LiCl [56], which showed that uncomplexed $NpO_2^+$ is the predominant Np(V) species for [$Cl^-$] ≤ 6 M, whereas the monochloro complex, $NpO_2(OH_2)_4Cl(aq)$, prevails only for [$Cl^-$] ≥ 7. In the following discussion of the pH dependence of the vis/NIR spectra, the uncomplexed $NpO_2^+$ aquo ion is therefore assumed to be the main unhydrolysed Np(V) species even in 5.0 M NaCl.

In the spectra of the untreated, alkaline sample aliquots, the absolute absorbance of unhydrolysed Np(V) at $\lambda$ = 980.2–981.0 nm systematically decreases with increasing $pH_m$ value, see Figures 2 and A1 in the Appendix. A plot of log $Abs_{980-981}$ vs. $pH_m$ yields a slope of –1.1 ± 0.1, as expected for the equilibrium between $NpO_2OH$(am, fresh) and $NpO_2^+$ according to equation 1.

The total contribution of Np(V) hydrolysis species is estimated by comparing the spectral features of the prominent Np(V) peak at $\lambda_{max}$ = 980.2–981.0 nm in the untreated alkaline and the corresponding acidified aliquot of a sample. Up to $pH_m \sim 9.5$, the differences in the molar extinction (and width) are <5%, i. e. more than 95% of the Np(V) is present as unhydrolysed $NpO_2^+$. For the respective most alkaline sample ($pH_m$ = 9.9–10.3 in 0.1–5.0 M

NaCl), the contribution of Np(V) hydrolysis species is between 7% and 20%, accordingly. A small shoulder at about $\lambda \sim 991$–$992$ nm (the absolute absorbance is about $5$–$8 \times 10^{-4}$ which is close to the detection limit of the vis/NIR device, $3 \pm 1 \times 10^{-4}$) is visible in all "alkaline spectra" but disappears upon acidification. For the same ionic strength, the absolute absorbance of the shoulder is constant, i. e. independent of the pH value in the samples. It can therefore be attributed to the first Np(V) hydrolysis species, $NpO_2OH(aq)$, as its concentration controlled by $NpO_2OH(am, fresh)$ is also independent of pH according to equation 2.[1]

## 3.3 Solid phase characterization

### 3.3.1 XRD, SEM–EDS and quantitative chemical analysis

XRD patterns collected for the Np(V) solid phases listed in Table 1 are shown in Figure 3. All green $NpO_2OH(am, fresh)$ solid samples are X-ray amorphous, and, accordingly, reveal non characteristic XRD patterns with extremely broad reflexes (no entry in the JCPDS database). The position of these broad peaks may roughly be indicative of nanocrystalline $Np_2O_5(cr)$ (JCPDS–File 18–0871), however given the broad spectral features this remains largely speculative. The amorphous character of green solid phases is further confirmed by SEM pictures (Figure 4, upper line).

White solid phases controlling the solubility of Np(V) above $pH_m \sim 11.5$ in 3.0 M and 5.0 M NaCl exhibit distinct XRD patterns with sharp reflexes corresponding to a crystalline structure. The JCPDS database gives no match for the diffractograms recorded for these compounds. SEM pictures of these phases show a well-defined platelet-like morphology. On the contrary, the white solid phase collected at $pH_m = 11.8$ in 1.0 M NaCl shows broad XRD patterns corresponding to an amorphous structure. This compound sets a greater Np(V) solubility compared to the crystalline phases forming at higher $pH_m$ or NaCl concentration, but incorporates a larger Na-content in its stoichiometry compared to the greenish material (see Table 3). These observations likely hint towards an intermediate product in the transformation of the amorphous $NpO_2OH(am, fresh)$ material into a crystalline Na–Np(V)–OH phase.

In spite of the similar needle-like structure (see SEM pictures in Figure 4, bottom line), the violet-pink solid phases controlling Np solubility in 1.0 and 5.0 M NaCl, respectively, have remarkably different XRD patterns (Figure 3). The XRD pattern of the former solid shows a perfect agreement with the structure of $NaNpO_2(OH)_2(cr)$ described by Almond and co-workers [37]. Note that the latter authors prepared the $NaNpO_2(OH)_2(cr)$ phase by hydrothermal reaction of Np(V) and 1 M NaOH. The solid phase obtained was mostly consisting of transparent magenta needles, similar in morphology and color to the solid phase characterized in the present study.

Np(V) shows a great affinity towards carbonate, which leads to the formation of strong aqueous complexes and moderately soluble solid compounds ([25, 29, 59, 62–64], among others). At low carbonate concentrations and weakly alkaline conditions ($m_{CO_3^{2-}} < 10^{-3}$ m; $pH_m < 10$ – depending upon NaCl/$NaClO_4$ concentration), [63] and [29] reported the solubility of Np(V) to be controlled by $NaNpO_2CO_3 \cdot 3.5H_2O(cr)$. Above this carbonate concentration, $Na_3NpO_2(CO_3)_2 \cdot nH_2O(cr)$ instead of $NaNpO_2CO_3 \cdot 3.5H_2O(cr)$ is responsible for the solubility control. As the samples were strictly prepared and kept under carbonate-free conditions in an Ar-glovebox, XRD patterns reported for $Na_{0.6}NpO_2(CO_3)_{0.8} \cdot 2.5H_2O(cr)$ [65], $NaNpO_2(CO_3) \cdot nH_2O(cr)$ ($n = 0$, 1, 2, 3, and 3.5, [61]), $Na_3NpO_2(CO_3)_2 \cdot nH_2O(cr)$ and $Na_4NpO_2(CO_3)_{2.5} \cdot nH_2O(cr)$ [66] as expected did not provide any positive match with the XRD data collected for white and pink solid phases. Reference XRD patters of $NaNpO_2CO_3 \cdot 3.5H_2O(cr)$ are exemplarily shown in Figure 3.

The Na:Np ratio in the selected solid phases is summarized in Table 3, as quantified by chemical analysis and SEM–EDS. Analytical errors in chemical analysis by LSC and ICP–OES can be safely considered below 10%, whereas uncertainty associated to SEM–EDS lies typically within 10–40% (as standard deviation of 10 individual measurements).

Table 3 shows that all white and pink solids have a high Na-content ($0.8 \leq$ Na:Np $\leq 1.6$). This is in good agreement with the $NaNpO_2(OH)_2(cr)$ structure identified in sample 7 by XRD. Unexpectedly, both chemical analysis and SEM–EDS confirm that Na is also present in comparatively minor amounts in the amorphous green phases (Na:Np $\leq 0.3$). The fraction of Na in these solid phases appears to be independent of NaCl concentration and $pH_m$ in the corresponding solubility sample. Furthermore, SEM–EDS confirms that no (or only a very minor fraction of) $Cl^-$ is present in the green precipitate, and thus that Na is associated to the Np solid phase and is not present as NaCl impurity.

1 Note that the first Np(V) carbonato complex, $NpO_2CO_3^-$, has evidently an absorbance at $\lambda = 991$ nm [57–59]. Although very close in position to the shoulder observed in the present work, we argue $NpO_2CO_3^-$ not to be responsible for this absorption (which further implies the presence of carbonate impurities in the system) as the expected pH dependence of the peak was not observed.

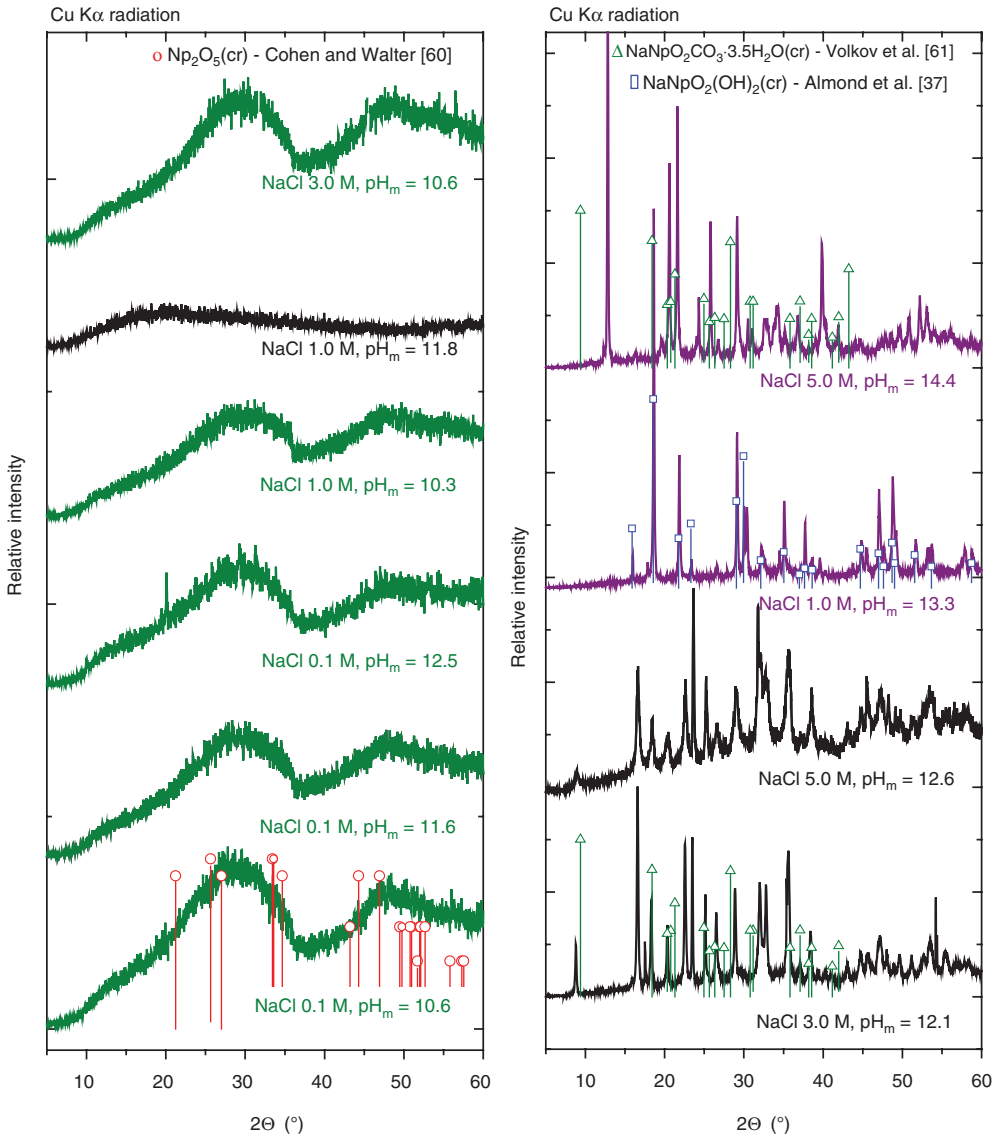



**Figure 3:** XRD spectra of selected solid phases from Np(V) solubility experiments in 0.1, 1.0, 3.0 and 5.0 M NaCl ($m_{NaCl}$ = 0.10, 1.02, 3.20 and 5.61 m). Green color of XRD spectra attributed to green solids, black color – to white solids, pink color – to pink solids. Circles, triangles and squares mark peak positions and relative intensities reported for $Np_2O_5$(cr) [60], $NaNpO_2CO_3 \cdot 3.5H_2O$(cr) [61] and $NaNpO_2(OH)_2$(cr) [37], respectively.

### 3.3.2 XANES and EXAFS

Figure 5 shows the XANES spectra of the solid phases described in Table 1. The comparison of these spectra with Np(IV), Np(V) and Np(VI) reference spectra reported elsewhere [67] clearly indicates that neptunium is predominantly found as +V in all solid phases characterized in this study.

Experimental and theoretical $k^2$-weighted Np $L_{III}$-edge EXAFS spectra and their corresponding Fourier transforms are shown in Figure 6. Structural parameters resulting from the fits are listed in Table 4. Note that for pink solid sample Nr. 7, the $k$ range was not sufficient to fit the data to the whole structure. Instead, only the shells corresponding to the main features were used, allowing the coordination number to vary.

The fit of EXAFS spectra of green solids in 0.1 M, 3.0 M and 5.0 M NaCl indicates the absence of Np–Np backscattering, as expected for amorphous structures. The distance determined for $Np–O_{eq}$ is in average longer than the distance recently reported for freshly precipitated $NpO_2OH$(am) in TMA–OH solutions (2.35 ± 0.03 Å) [67].

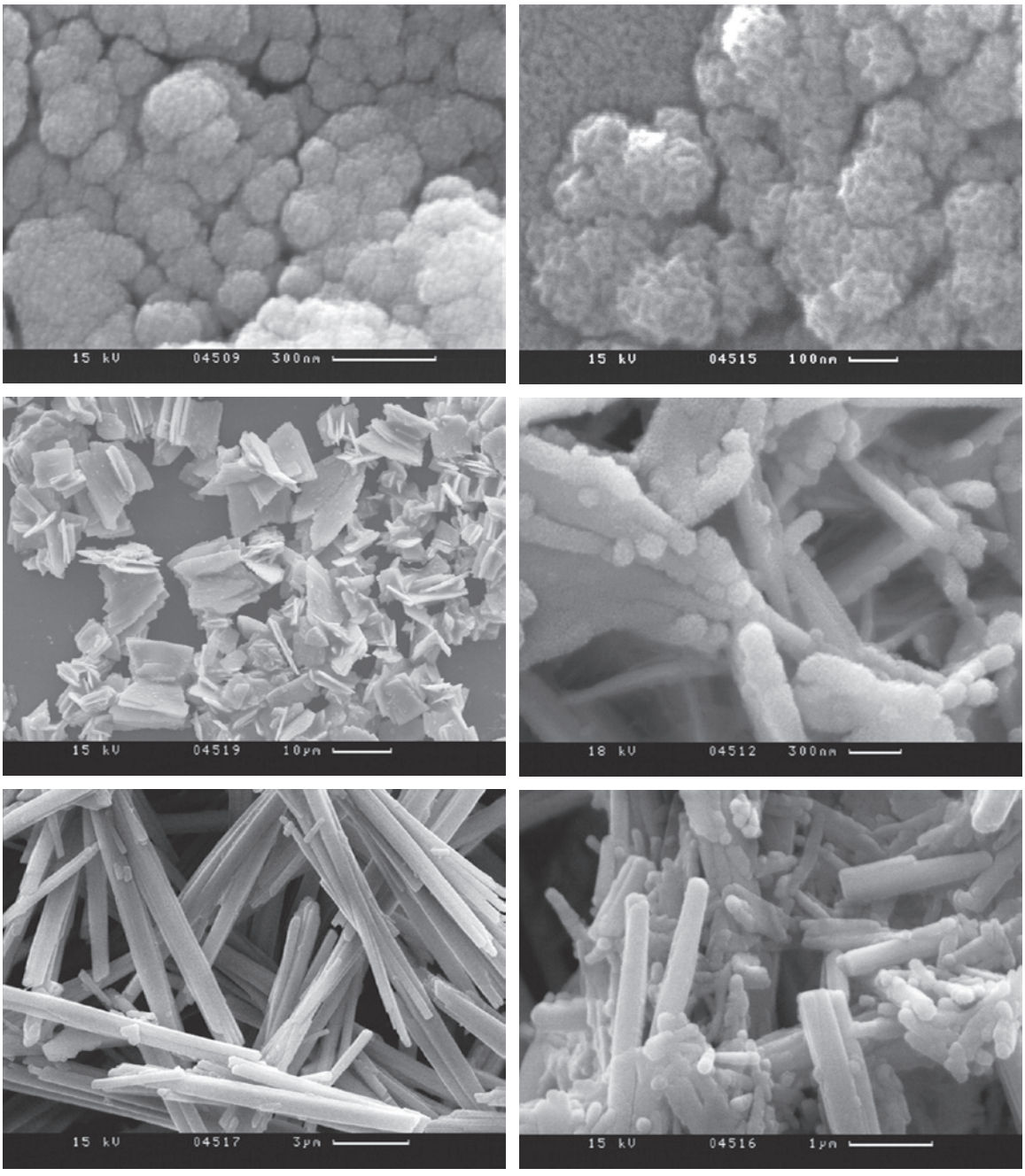



**Figure 4:** SEM images of the Np(V) solid phases controlling the solubility in NaCl solutions. Upper line: green solids (samples 2 and 8, respectively); middle line: white solids (samples 6 and 12); bottom line: violet-pink solids (samples 7 and 13).

This difference likely reflects slight modifications in the solid crystallinity between a solid phase aged 7 days [67] and ~2 years (present work).

High quality EXAFS spectra up to $k$ ~14 Å$^{-1}$ were collected for green solids in 0.1 M NaCl (samples 2 and 4). The fit of these EXAFS data is improved by the incorporation of Na-shells with relatively low coordination numbers and large Debye–Waller factors. This observation is in agreement with chemical analysis and SEM–EDS data.

Both Na- and Np-backscattering atoms are required to fit the EXAFS spectra collected from white and pink neptunium solids. This observation confirms that Na belongs in both cases to the structure of the neptunium solid phase and that both structures are well-ordered and rather crystalline. Nevertheless, the fit of EXAFS

**Table 3:** Na:Np ratio determined in selected Np(V) solid phases by quantitative chemical analysis and SEM–EDS.

| Sample | Ionic strength [M] | $pH_m$ | Color | Na:Np ratio | |
|---|---|---|---|---|---|
| | | | | Chemical analysis | SEM–EDS |
| 1 | 0.1 | 9.4 | Green | – | – |
| 2 | 0.1 | 10.6 | Green | 0.2 | 0.1 |
| 3 | 0.1 | 11.6 | Green | 0.2 | 0.2 |
| 4 | 0.1 | 12.5 | Green | 0.3 | 0.1 |
| 5 | 1.0 | 10.3 | Green | 0.3 | 0.2 |
| 6 | 1.0 | 11.8 | White | 0.8 | 0.6 |
| 7 | 1.0 | 13.3 | Violet-pink | 1.1 | 0.9 |
| 8 | 3.0 | 10.6 | Green | – | 0.3 |
| 9 | 3.0 | 12.1 | White | 0.8 | 0.7 |
| 10 | 5.0 | 9.6 | Green | – | – |
| 11 | 5.0 | 11.2 | Green | – | 0.2 |
| 12 | 5.0 | 12.6 | White | 1.6 | 1.0 |
| 13 | 5.0 | 14.4 | Violet-pink | 1.1 | 0.8 |

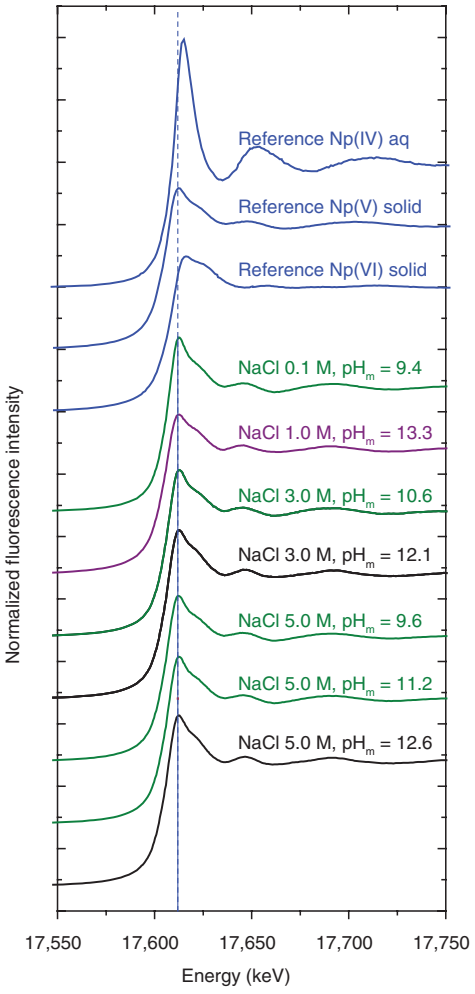



**Figure 5:** Experimental Np $L_{III}$ XANES spectra collected in this work for neptunium solid phases in alkaline NaCl solutions compared to Np(IV), Np(V) and Np(VI) reference spectra reported in [67].

spectra reflects major differences between the structures of both solid phases. In the first case, a successful fit is obtained based on the crystalline structure of $Na_2U_2O_7$(cr) ('diuranate' structure), where the central U-atom was substituted by Np. The structural parameters determined are very similar for white solids in 3.0 M and 5.0 M NaCl with Na- and Np-backscatterers at distances of 3.84 Å and 3.91–3.93 Å, respectively. Despite sharing a similar structure, distances Np(V)–$O_{ax}$ and Np(V)–$O_{eq}$ determined in this work (1.83 Å and 2.38–2.39 Å) differ significantly from those originally resolved by XRD for $Na_2U_2O_7$(cr) (1.92 Å and 2.31 Å). This is mostly due to the differences in effective charge between $NpO_2^+$ ($Z_{eff} = 2.3$) and $UO_2^{2+}$ ($Z_{eff} = 3.2$) cations [68, 69] and the implications of this difference on the electrostatic interaction taking place between $AnO_2^{n+}$ and OH/O–ligands in the equatorial plane.

EXAFS spectra of pink solids in samples 7 and 13 (see Table 1) could not be fitted on the basis of the $Na_2U_2O_7$(cr) structure. Instead, a successful and stable fit is obtained using the cif structure of $NaNpO_2(OH)_2$(cr) as reported in Almond et al. [37]. This is consistent with the positive match obtained for the XRD pattern of sample 7 and XRD data reported by Almond and co-workers (see Section 3.2.1). The structure reported by these authors is a three-dimensional net built from chains connected through bridging hydroxyl group $[Np^VO_2]O(OH)_4$ bipyramids, whereas $Na_2U_2O_7$(cr) (and by turn the white Np(V) phase characterized in the present work) has a layered structure with Na-atoms allocated in the interlayer.

Although the EXAFS spectra of both pink samples can be fitted based on the crystalline structure of $NaNpO_2(OH)_2$(cr) resolved by Almond and co-workers, the resulting structural parameters summarized in Table 4 show significant differences. This disagreement confirms the differences observed in the corresponding XRD patterns (Section 3.3.1) also pointing towards markedly different structural characteristics.

## 3.4 Implications of the newly generated data on the Np(V) thermodynamic model in NaCl systems

### 3.4.1 Hydrolysis of Np(V)

Thermodynamic data selection provided in the NEA–TDB for the hydrolysis of Np(V) relies on solubility measurements over uncharacterized $NpO_2OH$(am) solid phases [28]. The NEA review team therefore acknowledged that the selected hydrolysis constants should be considered with caution. Thermodynamic calculations using the

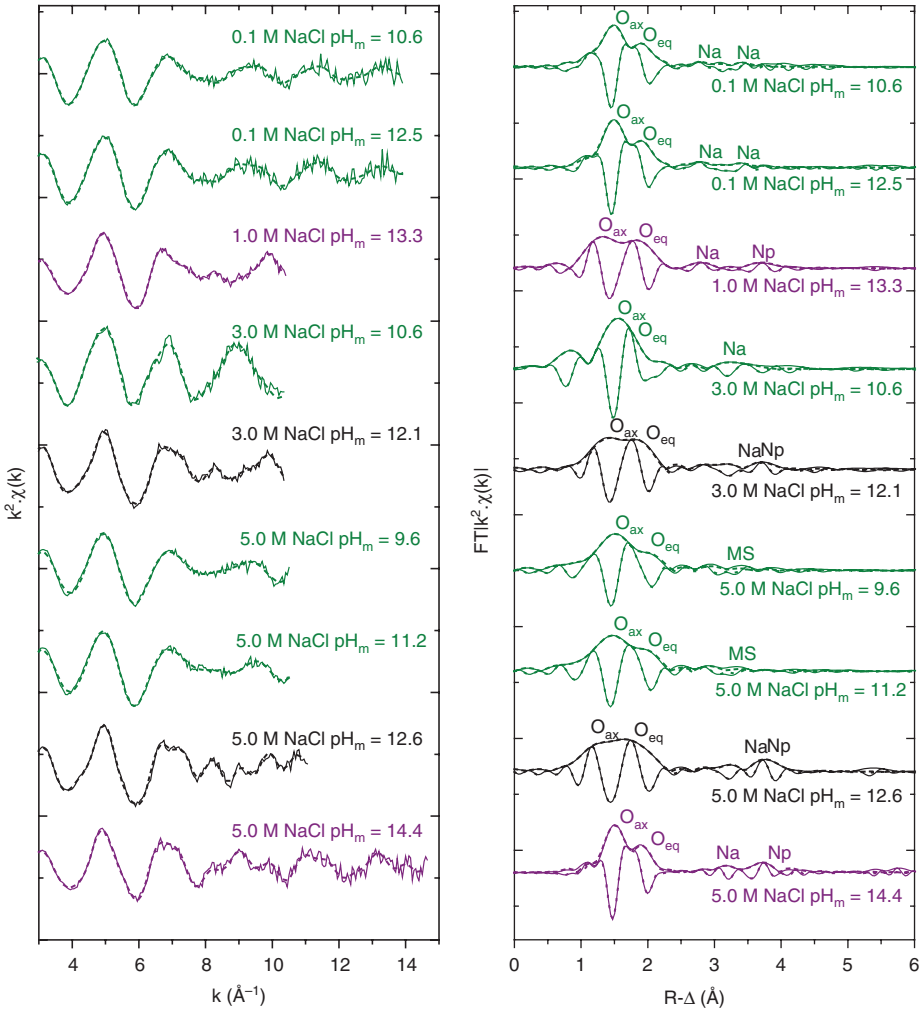



**Figure 6:** Experimental (solid line) and theoretical (dashed and dotted lines) (left) k$^2$-weighted Np L$_{III}$-edge EXAFS spectra and (right) corresponding Fourier Transform (modulus and imaginary parts) for solid phases controlling the solubility of Np(V) in alkaline 0.1 M–5.0 M NaCl solutions.

NEA–TDB selection predict the predominance of $NpO_2^+$ below $pH_m \sim 11$ (solid lines in Figure 7).

A number of publications using various experimental techniques (potentiometry, spectrophotometry, solubility) and reporting greater hydrolysis constants were disregarded in [7] because of the likely contribution of Np(V)–carbonate species or unaccounted precipitation of $NpO_2OH(am)$ ([23–25], among others). After the release of the last NEA–TDB update book [8], Rao and co-workers [30] comprehensively assessed the hydrolysis of Np(V) at different temperatures using a combination of potentiometric, spectrophotometric and microcalorimetric techniques. The stability constants derived by these authors for the first and second hydrolysis species of Np(V) are more than two orders of magnitude greater than those selected in [7], and thus predict the predominance of $NpO_2OH(aq)$ and $NpO_2(OH)_2^-$ at $pH_m$ above ~9 (dashed lines in Figure 7[2]).

The fraction of $NpO_2^+$ at $pH_m \leq 10.3$ quantified in the present work by UV-vis/NIR spectroscopy (see Section 3.2) is shown in Figure 7 for the systems 0.1, 1.0, 3.0 and 5.0 M NaCl. These data are consistent with thermodynamic calculations based on the NEA–TDB selection, and clearly disregard an earlier onset of the Np(V) hydrolysis as predicted using the hydrolysis constants reported in [30]. Although Rao and co-workers took great care in their

**2** Calculations in Figure 7 are performed with NaCl as background electrolyte and considering SIT ion interaction coefficients for Np(V) species reported in the NEA–TDB. Although experiments in [30] were conducted in 1.0 M tetramethylammonium chloride (TMA–Cl), these authors considered $\varepsilon(X^-, TMA^+) \approx \varepsilon(X^-, Na^+)$.

**Table 4:** Structural parameters determined for solid phases controlling Np(V) solubility in 0.1 M–5.0 M NaCl.

| Sample | Backscatterer | $R^a$ (Å) | $N^b$ | $\sigma^2$(Å$^2$) | $\Delta E_0$ (eV) | *R*-factor |
|---|---|---|---|---|---|---|
| Green solid (Nr. 2) | $O_{ax}$ | 1.86 | 1.2 | 0.002 | 9.0 | 0.4 |
| $I$ = 0.1 M NaCl, $pH_m$ = 10.6 | $O_{eq}$ | 2.43 | 3.8 | 0.013 | 9.0 | |
| (2.5 ≤ $k$ [Å$^{-1}$] ≤ 13.9) | Na | 3.32 | 1.8 | 0.015 | 3.0 | |
| | Na | 3.97 | 0.7 | 0.001 | 3.0 | |
| Green solid (Nr. 4) | $O_{ax}$ | 1.87 | 1.2 | 0.001 | 7.9 | 0.4 |
| $I$ = 0.1 M NaCl, $pH_m$ = 12.5 | $O_{eq}$ | 2.42 | 4.5 | 0.013 | 7.9 | |
| (2.5 ≤ $k$ [Å$^{-1}$] ≤ 13.9) | Na | 3.29 | 2.3 | 0.015 | 1.6 | |
| | Na | 3.97 | 1.1 | 0.001 | 1.6 | |
| Pink solid (Nr. 7) | $O_{ax}$ | 1.82 | 2.1 | 0.008 | 0.6 | 0.04 |
| $I$ = 1.0 M NaCl, $pH_m$ = 13.3 | $O_{eq}$ | 2.40 | 4.0 | 0.008 | 0.6 | |
| (2.6 ≤ $k$ [Å$^{-1}$] ≤ 10.3) | Na | 3.30 | 0.7 | 0.003 | −5.0 | |
| | Np | 3.90 | 1.4 | 0.006 | 3.4 | |
| Green solid (Nr. 8) | $O_{ax}$ | 1.89 | 1.8 | 0.001 | 2.2 | 0.4 |
| $I$ = 3.0 M NaCl, $pH_m$ = 10.6 | $O_{eq}$ | 2.35 | 6.0 | 0.013 | 2.2 | |
| (3.1 ≤ $k$ [Å$^{-1}$] ≤ 10.0) | Na | 3.92 | 2.1 | 0.002 | −0.9 | |
| White solid (Nr. 9) | $O_{ax}$ | 1.83 | 2* | 0.005 | 5.0 | 0.4 |
| $I$ = 3.0 M NaCl, $pH_m$ = 12.1 | $O_{eq}$ | 2.38 | 6* | 0.009 | 5.0 | |
| (2.7 ≤ $k$ [Å$^{-1}$] ≤ 10.3) | Na | 3.84 | 6* | 0.005 | −3.8 | |
| $S_0^2$ = 0.5 | Np | 3.91 | 6* | 0.017 | 4.8 | |
| Green solid (Nr. 10) | $O_{ax}$ | 1.83 | 1.3 | 0.002 | 0.38 | 0.9 |
| $I$ = 5.0 M NaCl, $pH_m$ = 9.6 | $O_{eq}$ | 2.40 | 5.4 | 0.015 | 0.38 | |
| (2.7 ≤ $k$ [Å$^{-1}$] ≤ 10.5) | MS | 3.65 | 1.4 | 0.006 | 0.38 | |
| Green solid (Nr. 11) | $O_{ax}$ | 1.81 | 1.3 | 0.0007 | −0.2 | 0.8 |
| $I$ = 5.0 M NaCl, $pH_m$ = 11.2 | $O_{eq}$ | 2.40 | 4.7 | 0.011 | −0.2 | |
| (2.7 ≤ $k$ [Å$^{-1}$] ≤ 10.5) | MS | 3.62 | 1.4 | 0.003 | −0.2 | |
| White solid (Nr. 12) | $O_{ax}$ | 1.83 | 2* | 0.006 | 5.1 | 0.3 |
| $I$ = 5.0 M NaCl, $pH_m$ = 12.6 | $O_{eq}$ | 2.39 | 6* | 0.009 | 5.1 | |
| (2.7 ≤ $k$ [Å$^{-1}$] ≤ 11.0) | Na | 3.84 | 6* | 0.017 | −3.5 | |
| $S_0^2$ = 0.61 | Np | 3.93 | 6* | 0.007 | 3.9 | |
| | O | 4.67 | 12* | 0.017 | 5.1 | |
| Pink solid (Nr. 13) | $O_{ax}$ | 1.88 | 2* | 0.001 | 6.9 | 1.1 |
| $I$ = 5.0 M NaCl, $pH_m$ = 14.4 | $O_{eq}$ | 2.39 | 5* | 0.007 | 6.9 | |
| (2.6 ≤ $k$ [Å$^{-1}$] ≤ 14.7) | Na | 3.30 | 1* | 0.002 | 6.9 | |
| $S_0^2$ = 0.619 | Na | 3.58 | 2* | 0.004 | 6.9 | |
| | Na | 3.88 | 2* | 0.001 | 6.9 | |
| | Np | 3.97 | 2* | 0.002 | 8.4 | |
| | Np | 4.13 | 2* | 0.004 | 8.4 | |

*Parameter fixed in the fit; [a]Uncertainty associated to $R$ is ±0.02 Å; [b]Uncertainty associated to $N$ is ±20%.

Amplitude reduction factor ($S_0^2$) fixed to 1.0 in all cases except indicated otherwise. Note that the amplitude of a given shell is given by $S_0^2 * N$ so that $N$ = 1.2 with $S_0^2$ = 1 is identical to $N$ = 2 with $S_0^2$ = 0.6 Values in brackets corresponding to the $k$-range considered for the EXAFS fit in each sample.

experimental approach, this discrepancy confirms the hypothesis of carbonate contamination during the titration experiment and consequent formation of $NpO_2CO_3^-$, with a reported absorption band at $\lambda$ = 991 nm ([57–59]; see also footnote 1).

In spite of the fair agreement with thermodynamic calculations using NEA–TDB, spectroscopic data collected in the present work support an earlier onset of Np(V) hydrolysis (*ca.* 0.2–0.3 $\log_{10}$-units), thus pointing to a slight overestimation of the first hydrolysis constant selected in [7].

An accurate evaluation of Np(V) aqueous speciation using UV-vis/NIR is not feasible beyond $pH_m$ ~10.5 (using standard 1 cm cuvettes) because of the low $m_{Np}$ imposed by $NpO_2OH$(am, fresh) (or additional ternary Na–Np(V)–OH phases forming). Hence, the Np(V) hydrolysis scheme

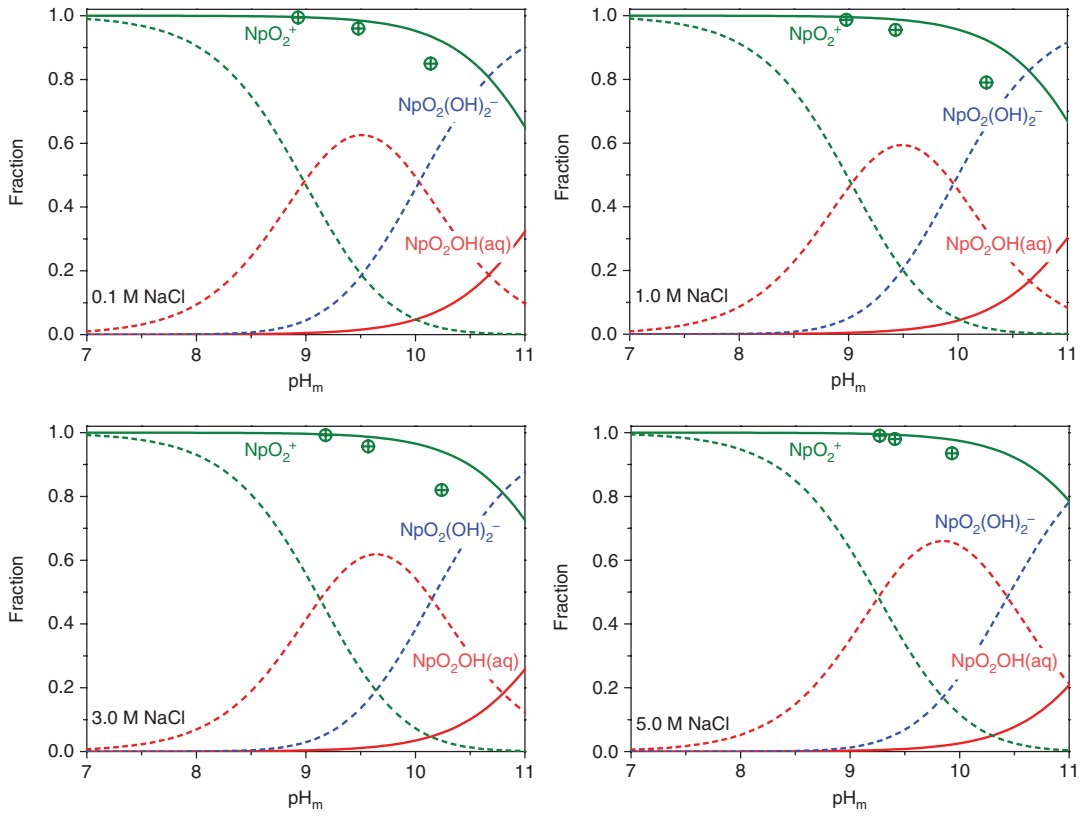



**Figure 7:** Fraction diagram of Np(V) within $7 \le pH_m \le 11$, as calculated using hydrolysis constants selected in the NEA–TDB (solid lines) and reported by Rao and co-workers ([30], dashed lines). Symbols ⊕ correspond to the fraction of $NpO_2^+$ quantified in the supernatant solution of selected solubility samples as the difference in intensity of the 980–981 nm NIR peak before and after acidification of the solution (see Section 3.2).

derived in [28] and later selected in the NEA–TDB [7] was based on the slope analysis of solubility data, and strongly relied on (i) the predominance of $NpO_2OH(am)$ over the complete pH range investigated (see discussion in Section 3.4.2) and (ii) the absence of other Np(V) aqueous species besides $NpO_2^+$ and $NpO_2(OH)_x^{1-x}$ (e. g. carbonate complexes). Carbonate impurities are ubiquitous in NaOH, even for high purity commercial reagents. The systematic increase in carbonate concentration with increasing $pH_m$ can lead to the misinterpretation of the experimental observations, if carbonate complexes of Np(V) instead of hydrolysis species form/dominate. In the present work, carbonate impurities are considered insufficient as to impact the aqueous chemistry of Np(V). Note that the highest carbonate concentration present in 0.1 M NaCl–NaOH solutions is $(3 \pm 1) \times 10^{-6}$ m (corresponding to 0.1 M NaOH), whereas $m_{Np}$ was quantified as $(5.6 \pm 0.6) \times 10^{-6}$ m for the same pH and background electrolyte concentration (see Figure 1). The excellent agreement between solubility data in dilute NaCl and $NaClO_4$ systems using two different commercial NaOH (Titrisol Merck in the present work, $CO_2$-free NaOH from Baker Co. in [28]) further argues in favor of the absence of carbonate impact on the Np(V) solubility data.

On the other hand, the interpretation of Np(V) aqueous speciation in concentrated NaCl systems (≥1.0 M) and $pH_m$ above ~13 is not straight forward. Because of the solubility control exerted by ternary Na–Np(V)–OH phases (see Section 3.3 and 3.4.2) and provided the absence of carbonate aqueous species, the increase in solubility observed for these systems and pH-region can only be explained by the formation of higher hydrolysis species ($Np^VO_2(OH)_x^{1-x}$ or $Np^{VI}O_2(OH)_x^{2-x}$ with $x \ge 3$). Tananaev [70, 71] reported the formation of the species $NpO_2(OH)_3^{2-}$ and $NpO_2(OH)_4^{3-}$ in alkaline NaOH and TMA–OH solutions based on UV-vis/NIR investigations. Note that the NIR peak at $\lambda = 1020$ nm attributed by Tananaev to $NpO_2(OH)_3^{2-}$ was later assigned to ternary Np(V)–OH–$CO_3$ species forming in carbonate bearing $NaClO_4$–NaOH [64] and TMA–Cl/OH solutions [67]. In alkaline concentrated $CaCl_2$ systems, Fellhauer and co-workers [38, 39] observed the formation of previously unreported Np(V) species containing the moiety $[NpO_2(OH)_5]^{4-}$. Such a negatively-charged moiety was stabilized in solution by the

inner-sphere coordination of three $Ca^{2+}$ atoms. It remains uncertain whether, under hyperalkaline conditions, alkali metals such as $Na^+$ can also stabilize these higher Np(V) hydrolysis species. The Np(V)–Np(VI) redox border in alkaline to hyperalkaline pH conditions was recently assessed by Gaona and co-workers [67, 72]. Based on the newly generated thermodynamic data for Np(VI) aqueous species, the authors defined a stability field of Np(V) under hyperalkaline conditions significantly smaller than previously assumed. The oxidation of Np(V)–Np(VI) and consequent predominance of $Np^{VI}O_2(OH)_4^{2-}$ in the aqueous phase could also explain the experimental observations described above. Data collected within this study or available from literature prove to be insufficient to validate any of these hypotheses.

### 3.4.2 Solubility of $NpO_2OH$(am, fresh) and formation of ternary Na–Np(V)–OH phases

Thermodynamic data currently selected in the NEA–TDB for the solubility of $NpO_2OH$(am, fresh) and hydrolysis constants of Np(V) explain properly (within the provided uncertainties) the experimental solubility data in both 0.1 M NaCl and $NaClO_4$ solutions within the $pH_m$ range 9–13 (solid line in Figure 1 upper left). Furthermore, the use of SIT ion interaction coefficients reported in the NEA–TDB allow to qualitatively explain the trend observed in this work for the solubility of Np(V) within 0.1 M ≤ $I$ (NaCl) ≤ 5.0 M and $pH_m \leq 11.5$. These calculations slightly overestimate Np(V) solubility at high NaCl concentrations, but agree with experimental data if considering the uncertainty reported in the NEA–TDB for $\varepsilon(NpO_2^+, Cl^-) = 0.09 \pm 0.05$ mol · $kg_w^{-1}$.

However, the observed high complexity of the Na–Np(V)–OH system in terms of solid phase formation well justifies doubts on the speciation scheme originally proposed by Neck and co-workers, which strongly relied on the predominance of the $NpO_2OH$(am) phase (either fresh or aged) over the entire $pH_m$ range 9–14. In the present work, the very well defined slope of –1 ($\log m_{Np}$ vs. $pH_m$) over ~1.5 $pH_m$-units in combination with the predominance of $NpO_2^+$ confirmed by UV-vis/NIR supports that equilibrium reaction (1) – $NpO_2OH(am, fresh) + H^+ \Leftrightarrow NpO_2^+ + H_2O$ – is controlling the solubility of Np(V) below $pH_m \sim 11$. In spite of this evidence, this hypothesis can be challenged by the non-stoichiometric presence of Na identified in the greenish phases controlling the solubility in 0.1 M NaCl (whole pH-range) and concentrated NaCl systems with $pH_m \leq 11.5$. Both the sorption of $Na^+$ on the surface of $NpO_2OH$(am, fresh) or the presence of minor amounts of a secondary Na–Np(V)–OH phase could explain the presence of Na in the green solid phases. In view of the structural parameters determined by EXAFS for Np(V) solid phases in dilute NaCl solutions (Table 4), the latter hypothesis arises as most likely. The incorporation or adsorption of minor amounts of foreign ions by amorphous actinide solid phases was previously discussed by Felmy and co-workers [73] in the framework of a solubility study with $ThO_2$(am) in saline systems. The authors proposed the incorporation of Na under formation of $Na_2ThO_3$(cr), but concluded that the presence of minor amounts of this crystalline phase, as well as $ThO_2$(cr), did not lead to a significant decrease in the solubility of Th(IV), which remained controlled by amorphous $ThO_2$(am). The same reasoning/hypothesis is raised in the present work to support $NpO_2OH$(am, fresh) as solubility controlling phase in the greenish amorphous material.

The results from the solubility experiments and the extensive solid phase analysis clearly indicate that a complete solid phase transformation takes place at $pH_m \geq 11.5$ and $I \geq 1.0$ M NaCl. Under these boundary conditions, the amorphous greenish material transforms into white and pinkish crystalline phases with a ratio 0.8 ≤ Na:Np ≤ 1.6. As indicated in Section 3.3.1, none of these phases is consistent with XRD patterns reported for Np(V) carbonate phases of the type $NaNpO_2CO_3 \cdot nH_2O$(cr).[3]

The crystal structure reported in [37] for the anhydrous $NaNpO_2(OH)_2$(cr) resulted in a positive match with XRD patterns collected for the Np(V) solid phase in 1.0 M NaCl and $pH_m = 13.3$. Note also that ternary phases of the type $Na_xNpO_2(OH)_{1+x} \cdot nH_2O$(cr) with $x = 1$–3 were previously synthesized by Tananaev using solid state reactions and precipitation from oversaturation conditions in aqueous systems (both at room temperature and hydrothermal conditions) [33–36]. For the synthetic approach at room temperature in 0.1–2.0 M NaOH solutions, Tananaev observed the predominant formation of $NaNpO_2(OH)_2 \cdot nH_2O$(cr) with the minor presence of $Na_2NpO_2(OH)_3 \cdot nH_2O$(cr) as impurity. These findings are consistent with the in-situ solid phase transformations observed in the present work, and confirm the relevant role of ternary Na–Np(V)–OH phases in controlling the

3 Indeed, the transformation of $NpO_2OH$(am, fresh) into $NaNpO_2CO_3 \cdot 3.5H_2O$(cr) in the conditions of this study can be also ruled out based on thermodynamic calculations. Considering the greatest carbonate concentration available in the 5.0 M NaCl–NaOH series ($3 \times 10^{-5}$ M in 1.0 M NaOH + 4.0 M NaCl), the solid phase transformation according with $NpO_2OH(am, fresh) + Na^+ + CO_3^{2-} + H^+ + 2.5H_2O \Leftrightarrow NaNpO_2CO_3 \cdot 3.5H_2O$(cr) is only expected at $pH_m \leq 10.6$.

solubility of neptunium in alkaline concentrated NaCl solutions.

The formation of a white binary $NpO_2OH$(am, aged) phase reported in previous solubility studies in concentrated $NaClO_4$ [28] and NaCl [29] solutions has not been observed in the present work. Hence, for those systems where no transformation to ternary Na–Np(V)–OH phases occurred, the solubility of $NpO_2OH$(am, fresh) remained unaltered within the timeframe of this study (2 years). A similar behavior of Np(V) solubility in dilute to concentrated NaCl systems was reported by Roberts and co-workers within an equilibration time of 37 days [51, 52]. Although differences between $NaClO_4$ and NaCl background electrolytes could justify the discrepancies with the observations reported by Neck et al. [28], we find no explanation for the disagreement with solubility data reported by Runde and co-workers [29].

## 4 Conclusions

The hydrolysis and solubility of Np(V) have been investigated in dilute to concentrated NaCl solutions within the $pH_m$ range 9–14. Special focus was given to the identification of the Np(V) solid phases controlling the solubility under different $pH_m$ and NaCl conditions, as well as to the correct account of the impact of carbonate on the evaluated systems. The newly generated data clearly show that the aqueous Np(V)–NaCl system exhibits a very complex chemical behavior, especially with regard to the solid phases controlling the solubility of Np. This is an interesting finding from the perspective of fundamental actinide chemistry, but also directly affects the chemical and thermodynamic models used to quantitatively describe this important sub-system of direct relevance for certain nuclear waste disposal scenarios.

The solubility curve of Np(V) in dilute NaCl systems has three well-defined regions with slopes ($\log_{10} m_{Np}$ vs. $pH_m$) of –1, 0 and +1. UV-vis/NIR confirms the predominance of $NpO_2^+$ in the first region, consistently with thermodynamic calculations using Np(V) hydrolysis constants selected in the NEA–TDB. This supports the hypothesis that the X-ray amorphous greenish phase $NpO_2OH$(am, fresh) controls the solubility under these conditions, in spite of the non-stoichiometric fraction of Na identified in the solid phase by quantitative chemical analysis, SEM–EDS and EXAFS. The same greenish material controls the solubility in concentrated NaCl solutions with $pH_m$ below ~11.5. In all these systems, $m_{Np}$ in equilibrium with $NpO_2OH$(am, fresh) remained unaltered within the timeframe of this study (2 years). Hence, no evidence of the aging of $NpO_2OH$(am, fresh) and consequent decrease in $m_{Np}$ has been observed in this work, in contrast with previous findings obtained in concentrated $NaClO_4$ and NaCl systems. The formation of crystalline ternary Na–Np(V)–OH phases with $0.8 \leq Na{:}Np \leq 1.6$ was confirmed by XRD, SEM–EDS, quantitative chemical analysis and EXAFS. These solid phases prevail in concentrated NaCl systems with $pH_m$ above ~11.5, and show significantly lower solubility than $NpO_2OH$(am, fresh). The increase in $m_{Np}$ in equilibrium with ternary Na–Np(V)–OH phases observed at $pH_m$ above ~12.5 is likely related with the formation of $Np^{V}O_2(OH)_x^{1-x}$ or $Np^{VI}O_2(OH)_x^{2-x}$ aqueous species with $x \geq 3$. Solubility and spectroscopic data collected within this study proves to be insufficient to validate any of these hypotheses.

Until resolving the uncertainties identified in the present work for ternary Na–Np(V)–OH phases and aqueous speciation in alkaline NaCl systems, we recommend the use of $NpO_2OH$(am, fresh) as Np(V) solubility-controlling phase in combination with the Np(V) hydrolysis scheme reported in the NEA–TDB for source term estimations as robust and defendable upper limit concentrations. Furthermore, we discourage the use of $\log_{10} {}^{*}K^{\circ}_{s,0}$ reported in the NEA–TDB for $NpO_2OH$(am, aged) for thermodynamics calculations in NaCl media, as this may result in underestimated Np(V) concentrations. Undersaturation solubility experiments with well-defined ternary Na–Np(V)–OH phases are on-going at KIT–INE to derive the thermodynamic properties of these solid phases and gain conclusive insights on the hydrolysis of Np(V) under hyperalkaline conditions.

**Acknowledgments:** M. Böttle and E. Soballa (KIT–INE) are kindly acknowledged for the performance of ICP–OES and SEM–EDS analyses. The research leading to these results has received funding from the European Union's European Atomic Energy Community's (Euratom) Seventh Framework Programme FP7/2007–2011 under grant agreement n° 212287 (RECOSY project). V.P. also acknowledges the German Academic Exchange Service (DAAD), Russian Science Foundation (project 16-13-00049) and ACTINET–i3 Integrated Infrastructure Initiative for financial support. ANKA (KIT Karlsruhe) is acknowledged for providing beamtime.

# Appendix

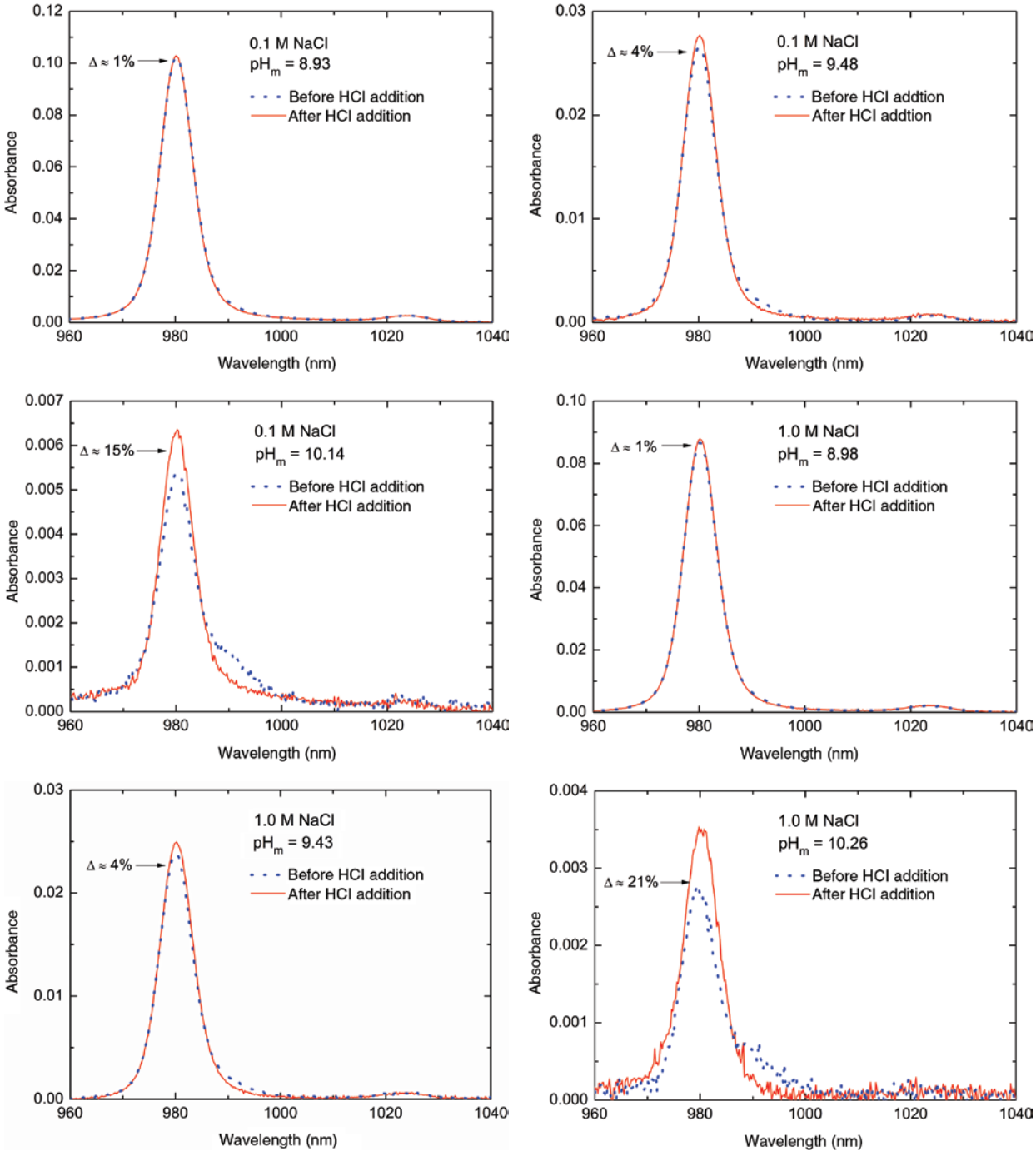



**Figure A1:** Near-IR absorption spectra of the saturated, supernatant solutions in equilibrium with $NpO_2OH$(am, fresh) in 0.1, 1.0, 3.0 and 5.0 M NaCl ($m_{NaCl}$ = 0.10, 1.02, 3.20 and 5.61 m). The vis/NIR sample aliquots were acidified in the cuvette with HCl after the measurement, and a second spectrum recorded. The total contribution of Np(V) hydrolysis species is estimated from the difference of the main peaks' heights ("Δ") in both spectra.

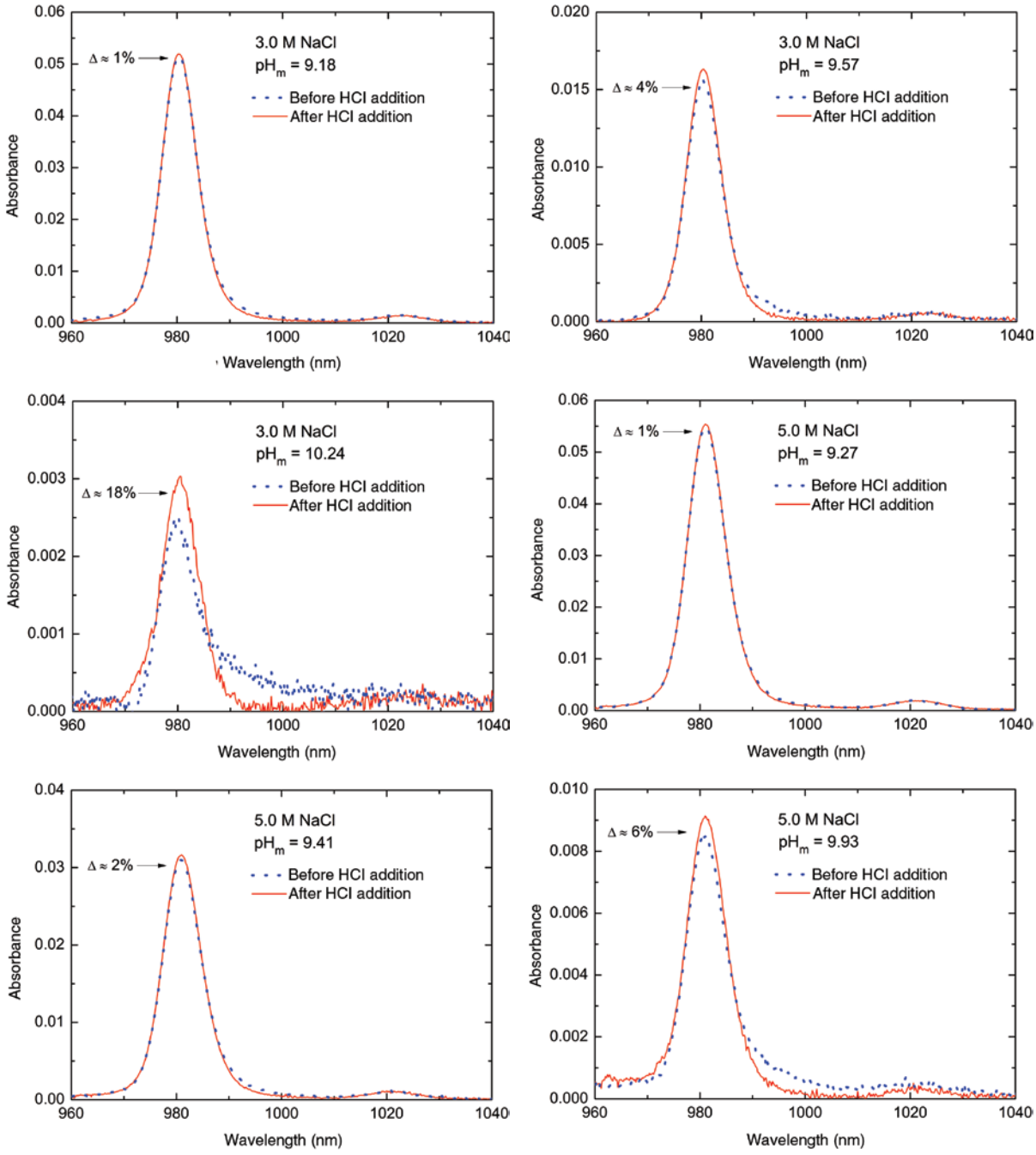



**Figure A1** (continued)

# References


1. Kaplan, D. I., Serne, R. J., Owen, A. T., Conca, J., Wietsa, T. W., Gervais, T. L.: Radionuclide adsorption distribution coefficients measured in Hanford sediments for the low level waste Performance Assessment project; PNNL–11485, Pacific Northwest Laboratory, (1996).
2. Kalmykov, S. N., Kriventsov, V. V., Teterin, Y. A., Novikov, A. P.: Plutonium and neptunium speciation bound to hydrous ferric oxide colloids. Cr. Chim. **10**, 1060 (2007).
3. Novikov, A. P., Malikov, D. A., Vinokurov, S. E., Kazinskaya, I. E., Goryachenkova, T. A., Myasoedov, B. F.: Concentration of neptunium from the ground waters of the Karachai Lake contamination area. J. Radioanal. Nucl. Ch. **289**, 431 (2011).
4. Kaszuba, J. P., Runde, W. H.: The aqueous geochemistry of neptunium: dynamic control of soluble concentrations with applications to nuclear waste disposal. Environ. Sci. Technol. **33**, 4427 (1999).
5. Altmaier, M., Vercouter, T.: Aquatic chemistry of the actinides: aspects relevant to their environmental behaviour. In: C. Poinssot, H. Geckeis (Eds.), Radionuclide Behaviour in the Natural

Environment: Science, Implications and Lessons for the Nuclear Industry (2012), Woodhead Publishing, Cambridge.
6. Altmaier, M., Gaona, X., Fanghänel, T.: Recent advances in aqueous actinide chemistry and thermodynamics. Chem. Rev. **113**, 901 (2013).
7. Lemire, R. J., Fuger, J., Nitsche, H., Potter, P. E., Rand, M. H., Rydberg, J., Spahiu, K., Sullivan, J. C., Ullman, W. J., Vitorge, P., Wanner, H.: Chemical Thermodynamics, vol. 4. Neptunium and Plutonium. (2001), (OECD, NEA-TDB) Elsevier, North Holland, Amsterdam.
8. Guillaumont, R., Fanghänel, J., Neck, V., Fuger, J., Palmer, D. A., Grenthe, I., Rand, M. H.: Chemical thermodynamics Vol. 5. Update on the Chemical Thermodynamics of Uranium, Neptunium, Plutonium, Americium and Technetium. (2003) (OECD, NEA-TDB) Elsevier, North Holland, Amsterdam.
9. Brown, P. L., Curti, E., Grambow, B.: Chemical thermodynamics, vol. 8. Chemical Thermodynamics of Zirconium. (2005) (OECD, NEA-TDB) Elsevier, North Holland, Amsterdam.
10. Gamsjäger, H., Bugajski, J., Gajda, T., Lemire, R., Preis, W.: Chemical thermodynamics, vol. 6. Chemical Thermodynamics of Nickel. (2005), (OECD, NEA-TDB) Elsevier, North Holland, Amsterdam.
11. Olin, A., Noläng, B., Öhman, L. O., Osadchii, E., Rosen, E.: Chemical Thermodynamics, vol. 7. Chemical Thermodynamics of Selenium. (2005), (OECD, NEA-TDB) Elsevier, North Holland, Amsterdam.
12. Rand, M., Fuger, J., Grenthe, I., Neck, V., Rai, D.: Chemical Thermodynamics, vol. 11. Chemical Thermodynamics of Thorium. (2009), (OECD, NEA-TDB) Elsevier, North Holland, Amsterdam.
13. Lemire, R. J., Berner, U., Musikas, C., Palmer, D. A., Taylor, P., Tochiyama, O.: Chemical Thermodynamics, vol. 13. Iron part I. (2013), (OECD, NEA-TDB) Elsevier, Paris.
14. Wieland, E., Van Loon, L. R.: Cementitious near-field sorption database for performance assessment of an ILW repository in Opalinus clay; Nagra Technical Report NTB 02-20, (2002), Nagra, Wettingen, Switzerland.
15. Gaona, X., Dähn, R., Tits, J., Scheinost, A. C., Wieland, E.: Uptake of Np(IV) by C-S-H phases and cement paste: an EXAFS study. Environ. Sci. Technol. **45**, 8765 (2011).
16. Tits, J., Gaona, X., Laube, A., Wieland, E.: Influence of the redox state on the neptunium sorption under alkaline conditions: batch sorption studies on titanium dioxide and calcium silicate hydrates. Radiochim. Acta **102**, 385 (2014).
17. Husar, R., Weiss, S., Hennig, C., Hubner, R., Ikeda-Ohno, A., Zanker, H.: Formation of Neptunium(IV)-Silica Colloids at Near-Neutral and Slightly Alkaline pH. Environ. Sci. Technol. **49**, 665 (2015).
18. Turner, D. R., Pabalan, R. T., Bertetti, F. P.: Neptunium(V) sorption on montmorillonite: an experimental and surface complexation modeling study. Clay Clay Miner. **46**, 256 (1998).
19. Bradbury, M. H., Baeyens, B.: Modelling the sorption of Mn(II), Co(II), Ni(II), Zn(II), Cd(II), Eu(III), Am(III), Sn(IV), Th(IV), Np(V) and U(VI) on montmorillonite: linear free energy relationships and estimates of surface binding constants for some selected heavy metals and actinides. Geochim. Cosmochim. Acta **69**, 875 (2005).
20. Wu, T., Amayri, S., Drebert, J., Van Loon, L. R., Reich, T.: Neptunium(V) sorption and diffusion in opalinus clay. Environ. Sci. Technol. **43**, 6567 (2009).
21. Amayri, S., Jermolajev, A., Reich, T.: Neptunium(V) sorption on kaolinite. Radiochim. Acta **99**, 349 (2011).
22. Frohlich, D. R., Amayri, S., Drebert, J., Reich, T.: Sorption of neptunium(V) on Opalinus Clay under aerobic/anaerobic conditions. Radiochim. Acta **99**, 71 (2011).
23. Kraus, K. A., Nelson, F.: The hydrolytic behavior of uranium and transuranic elements. Tech. Rep. AECD-1864, (1948), Oak Ridge National Laboratory, Oak Ridge, Tennesse.
24. Sevost'yanova, E. P., Khalturin, G. V.: Hydrolytic behavior of neptunium(V). Sov. Radiochem. **18**, 738 (1976).
25. Maya, L.: Hydrolysis and carbonate complexation of dioxoneptunium(V) in 1.0 M NaClO4 at 25°C. Inorg. Chem. **22**, 2093 (1983).
26. Nagasaki, Y., Shimidzu, H., Tsuruta, T.: A novel synthesis of omega-(4-vinylphenyl)alkanols. Makromol. Chem.-Rapid **9**, 381 (1988).
27. Itagaki, H., Nakayama, S., Tanaka, S., Yamawaki, M.: Effect of ionic-strength on the solubility of neptunium(V) hydroxide. Radiochim. Acta **58-9**, 61 (1992).
28. Neck, V., Kim, J. L., Kanellakopulos, B.: Solubility and hydrolysis behavior of neptunium(V). Radiochim. Acta **56**, 25 (1992).
29. Runde, W., Neu, M. P., Clark, D. L.: Neptunium(V) hydrolysis and carbonate complexation: experimental and predicted neptunyl solubility in concentrated NaCl using the Pitzer approach. Geochim. Cosmochim. Acta **60**, 2065 (1996).
30. Rao, L. F., Srinivasan, T. G., Garnov, A. Y., Zanonato, P. L., Di Bernardo, P., Bismondo, A.: Hydrolysis of neptunium(V) at variable temperatures (10–85 degrees C). Geochim. Cosmochim. Acta **68**, 4821 (2004).
31. Neck, V.: Comment on "Hydrolysis of neptunium(V) at variable temperatures (10–85 degrees C)" by L. Rao, T. G. Srinivasan, A. Yu. Garnov, P. Zanonato, P. Di Bernardo, and A. Bismondo. Geochim. Cosmochim. Acta **70**, 4551 (2006).
32. Rao, L. F., Srinivasan, T. G., Garnov, A. Y., Zanonato, P., Di Bernardo, P., Bismondo, A.: Response to the comment by V. Neck on "Hydrolysis of neptunium(V) at variable temperatures (10–85 degrees C)", Geochimica et Cosmochimica Acta 68, 4821–4830. Geochim. Cosmochim. Acta **70**, 4556 (2006).
33. Tananaev, I. G.: New Np(V) hydroxide compounds. Radiokhimiya **33**, 72 (1991).
34. Tananaev, I. G.: Preparation and characterization of neptunium(V) and americium(V) hydroxide compounds. Radiokhimiya **33**, 24 (1991).
35. Tananaev, I. G.: Solid state reactions of certain neptunium(V) compounds with bases. Radiokhimiya **33**, 19 (1991).
36. Tananaev, I. G.: Solid state transformations of neptunium(V) compounds in basic and carbonate media. Radiokhimiya **33**, 15 (1991).
37. Almond, P. M., Skanthakumar, S., Soderholm, L., Burns, P. C.: Cation-cation interactions and antiferromagnetism in Na[Np(V)$O_2(OH)_2$]: synthesis, structure, and magnetic properties. Chem. Mater. **19**, 280 (2007).
38. Fellhauer, D., Rothe, J., Altmaier, M., Neck, V., Runke, J., Wiss, T., Fanghänel, T.: Np(V) solubility, speciation and solid phase formation in alkaline $CaCl_2$ solutions. Part I: Experimental results. Radiochim. Acta **104**, 355 (2016).
39. Fellhauer, D., Altmaier, M., Gaona, X., Lützenkirchen, J., Fanghänel, T.: Np(V) solubility, speciation and solid phase formation in alkaline $CaCl_2$ solutions. Part II: Thermodynamics and implica-

tions for source term estimations of nuclear waste disposal. Radiochim. Acta **104**, 381 (2016).
40. Altmaier, M., Neck, V., Fanghänel, T.: Solubility of Zr(IV), Th(IV) and Pu(IV) hydrous oxides in $CaCl_2$ solutions and the formation of ternary Ca-M(IV)-OH complexes. Radiochim. Acta **96**, 541 (2008).
41. Neck, V., Altmaier, M., Rabung, T., Lützenkirchen, J., Fanghänel, T.: Thermodynamics of trivalent actinides and neodymium in NaCl, $MgCl_2$, and $CaCl_2$ solutions: solubility, hydrolysis, and ternary Ca-M(III)-OH complexes. Pure Appl. Chem. **81**, 1555 (2009).
42. Fellhauer, D., Neck, V., Altmaier, M., Lützenkirchen, J., Fanghänel, T.: Solubility of tetravalent actinides in alkaline $CaCl_2$ solutions and formation of $Ca_4[An(OH)_8]^{4+}$ complexes: a study of Np(IV) and Pu(IV) under reducing conditions and the systematic trend in the An(IV) series. Radiochim. Acta **98**, 541 (2010).
43. Jackson, N., Short, J. F.: The separation of neptunium and plutonium by ion exchange; AERE-M-444. (1959), Atomic Energy Research Establishment, England, Berks, Harwell.
44. Altmaier, M., Metz, V., Neck, V., Müller, R., Fanghänel, T.: Solid-liquid equilibria of $Mg(OH)_2$(cr) and $Mg_2(OH)_3Cl\ 4H_2O$(cr) in the system Mg-Na-H-OH-O-Cl-$H_2O$ at 25 degrees C. Geochim. Cosmochim. Acta **67**, 3595 (2003).
45. Rothe, J., Butorin, S., Dardenne, K., Denecke, M. A., Kienzler, B., Löble, M., Metz, V., Seibert, A., Steppert, M., Vitova, T., Walther, C., Geckeis, H.: The INE-Beamline for actinide science at ANKA. Rev. Sci. Instrum. **83**, 043105 (2012).
46. Denecke, M. A., Rothe, J., Dardenne, K., Blank, H., Hormes, J.: The INE-beamline for actinide research at ANKA. Phys. Scripta **T115**, 1001 (2005).
47. Newville, M.: EXAFS analysis using FEFF and FEFFIT. J. Synchrotron Radiat. **8**, 96 (2001).
48. Ravel, B., Newville, M.: ATHENA, ARTEMIS, HEPHAESTUS: data analysis for X-ray absorption spectroscopy using IFEFFIT. J. Synchrotron Radiat. **12**, 537 (2005).
49. Kovba, L. M., Ippolitova, E. A., Simanov, Y. P.: An X-ray study on alkali metal uranates. Doklady Akademii. Nauk. **120**, 1042 (1958).
50. Lierse, C., Treiber, W., Kim, J. I.: Hydrolysis reactions of neptunium(V). Radiochim. Acta **38**, 27 (1985).
51. Novak, C. F., Roberts, K. E.: Thermodynamic modeling of neptunium(V) solubility in concentrated Na-CO3-HCO3-Cl-ClO4-H-OH-H2O systems. Mater. Res. Soc. Symp. Proc. **353**, 1119 (1995).
52. Roberts, K. E., Silber, H. B., Torretto, P. C., Prussin, T., Becraft, K., Hobart, D. E., Novak, C. F.: The experimental determination of the solubility product for NpO2OH in NaCl solutions. Radiochim. Acta **74**, 27 (1996).
53. Hagan, P. G., Clevelan, J. M.: Absorption spectra of neptunium ions in perchloric acid solution. J. Inorg. Nucl. Chem. **28**, 2905 (1966).
54. Runde, W., Kim, J. I.: Untersuchung der Übertragbarkeit von Labordaten auf natürliche Verhältnisse. Chemisches Verhalten von drei und fünfwertigem Americium in salinen NaCl Lösungen; Report RCM 01094, TU München, München (1994).
55. Neck, V., Fanghänel, T., Rudolph, G., Kim, J. I.: Thermodynamics of neptunium(V) in concentrated salt-solutions – chloride complexation and ion-interaction (Pitzer) parameters for the $NpO_2^+$ ion. Radiochim. Acta **69**, 39 (1995).
56. Allen, P. G., Bucher, J. J., Shuh, D. K., Edelstein, N. M., Reich, T.: Investigation of aquo and chloro complexes of $UO_2^{2+}$, $NpO_2^+$, $Np^{4+}$, and $Pu^{3+}$ by X-ray absorption fine structure spectroscopy. Inorg. Chem. **36**, 4676 (1997).
57. Nitsche, H., Standifer, E. M., Silva, R. J.: Neptunium(V) complexation with carbonate. Lanthanide Actinide Res. **3**, 203 (1990).
58. Riglet, C.: Chimie du Neptunium et autres Actinides en milieu carbonate; Rapport CEA-R-5535, CEA, (1990), Fontenay aux Roses.
59. Neck, V., Runde, W., Kim, J. I., Kanellakopulos, B.: Solid-liquid equilibrium reactions of neptunium(V) in carbonate solution at different ionic strength. Radiochim. Acta **65**, 29 (1994).
60. Cohen, D., Walter, A. J.: Neptunium Pentoxide. J. Chem. Soc. 2696 (1964).
61. Volkov, Y. F., Visyachscheva, G. I., Kapshukov, I. I.: Studying carbonate compounds of pentavalent actinoids with alkali metal cations. Radiokhimiya **19**, 319 (1977).
62. Grenthe, I., Robouch, P., Vitorge, P.: Chemical-equilibria in actinide carbonate systems. J. Less.-Common Met. **122**, 225 (1986).
63. Neck, V., Runde, W., Kim, J. I.: Solid-liquid equilibria of neptunium(V) in carbonate solutions of different ionic strengths. 2. Stability of the solid-phases. J. Alloy Compd. **225**, 295 (1995).
64. Neck, V., Fanghänel, T., Kim, J. I.: Mixed hydroxo-carbonate complexes of neptunium(V). Radiochim. Acta **77**, 167 (1997).
65. Volkov, Y. F., Visyashcheva, G. I., Tomilin, S. V., Spiryakov, V. I., Kapshukov, I. I., Rykov, A. G.: Investigation of carbonate compounds of pentavalent actinides with alkali metal cations. Radiokhimiya **21**, 673 (1979).
66. Volkov, Y. F., Visyachscheva, G. I., Tomilin, S. V., Kapshukov, I. I., Rykov, A. G.: X-ray diffraction analysis of composition and crystal structure of some pentavalent actinide carbonates. (1979), NIIAR, USSR, Dimitrovgrad.
67. Gaona, X., Tits, J., Dardenne, K., Liu, X., Rothe, J., Denecke, M. A., Wieland, E., Altmaier, M.: Spectroscopic investigations of Np(V/VI) redox speciation in hyperalkaline TMA-(OH,Cl) solutions. Radiochim. Acta **100**, 759 (2012).
68. Choppin, G. R.: Utility of oxidation state analogs in the study of plutonium behavior. Radiochim. Acta **85**, 89 (1999).
69. Choppin, G. R., Rizkalla, E. N.; Solution chemistry of actinides and lanthanides. In: K. A. Gschneidner Jr., L. Eyring, (eds.), Handbook on the Physics and Chemistry of Rare Earths (1994), North Holland, Amsterdam.
70. Tananaev, I. G.: Forms of Np(V) and Am(V) in basic aqueous media. Radiokhimiya **32**, 53 (1990).
71. Tananaev, I. G.: Speciation of Np(V) in solutions of tetramethylammonium hydroxides. Radiokhimiya **36**, 15 (1994).
72. Gaona, X., Fellhauer, D., Altmaier, M.: Thermodynamic description of Np(VI) solubility, hydrolysis, and redox behavior in dilute to concentrated alkaline NaCl solutions. Pure Appl. Chem. **85**, 2027 (2013).
73. Felmy, A. R., Rai, D., Mason, M. J.: The solubility of hydrous thorium(Iv) oxide in chloride media – development of an aqueous ion-interaction model. Radiochim. Acta **55**, 177 (1991).